POLITECNICO DI TORINO

Master's Degree in Biomedical Engineering

Master's Degree Thesis

Nanostructured ferrite-based non-enzymatic electrochemical sensors for drug detection

Supervisors
Prof. Alberto Tagliaferro (PoliTo)
Prof. Sandro Carrara (EPFL)
Dr. Mattia Bartoli (IIT)

Candidate
Alessia Costanzo

Academic Year 2023-2024

Abstract

The advancement in nanotechnology has encouraged research into their application across various fields, including medical diagnosis. A currently expanding research area involves the utilization of nanomaterials in the development of electrochemical sensors for drug detection. This study focuses on the feasibility of using nano-oxides, specifically zinc ferrite, copper ferrite, and cobalt ferrite, in the fabrication of non-enzymatic electrochemical sensors to enhance the detection capabilities of paracetamol and cyclophosphamide.

The ferrites, synthesized via the autocombustion method, underwent characterization utilizing Raman spectroscopy and field emission scanning electron microscopy to verify their synthesis accuracy and probe their morphological attributes, respectively. The synthesized ferrites manifested uniform morphology, with dimensions ranging between 30 to 60 nm. These materials were subsequently utilized to functionalize the working electrode of commercially available screen-printed carbon electrodes through drop-casting technique.

Performance evaluation of the new sensors was conducted via cyclic voltammetry measurements, comparing the results with those obtained with a bare sensor.
Regarding paracetamol detection, the modified sensors exhibited a significant increase in oxidation current upon exposure to a 1.0 mM paracetamol solution, confirming the advancement in analytical performance.
Investigation into the kinetics of redox reactions, by varying the scan rate from 50 mV/s to 300 mV/s, revealed the presence of freely diffusing quasi-reversible systems. Exploiting the Laviron model and the Randles-Sevčik equation, the electron transfer coefficient, kinetic constant rate, and diffusion coefficient were determined.
Variations in paracetamol solution concentration from 0.5 mM to 3.0 mM allowed the derivation of the calibration curves, sensitivity and limit of detection (LoD). Compared to the unmodified sensor, characterized by a sensitivity of 24.1 $\pm$ 0.3 µA/mM and a LoD of 4.4 $\pm$ 0.1 µM, the modified sensors exhibited enhanced performance. Notably, zinc ferrite modified sensor yielded the best performing results, with a sensitivity of 28.3 $\pm$ 0.4 µA/mM and a LoD of 2.1 $\pm$ 0.1 µM.

In the case of cyclophosphamide detection, varying the concentration of the cyclophosphamide solution (10, 50, 100 µM) enabled the derivation of calibration curves, sensitivity, and detection limit. Compared to the unmodified sensor, which exhibited no detection capability at these low concentrations of cyclophosphamide solution, the sensor modified with copper ferrite demonstrated better and consistent performance, with a sensitivity of 20.2 $\pm$ 1.3 nA/µM and a LoD of 8.1 $\pm$ 0.5 µM.

In conclusion, this study highlights the significant potential of these materials in enhancing sensor efficacy. Promising prospects suggest the need for further investigations and research on other pharmaceutical compounds to broaden the application of these materials in the sensing and biosensing field.

Table of Contents

List of Tables

List of Figures

Acronyms

CE Counter Electrode

CNT Carbon Nanotube

CP Cyclophosphamide

CPE Carbon Paste Electrode

CV Cyclic Voltammetry

CYP Cytochrome

CYP450 Cytochrome P450

DI Deionized

DPV Differential Pulse Voltammetry

FAD Flavin Adenine Dinucleotide

FESEM Field Emission Scanning Electron Microscope

GCE Glassy Carbon Electrode

GOx Glucose Oxidase

Gr Graphene

HOMO Highest Occupied Molecular Orbital

IR Infrared

LoD Limit of Detection

LUMO Lowest Unoccupied Molecular Orbital

MWCNT Multi-Walled Carbon Nanotube

NM Nanomaterial

NP Nanoparticle

PBS Phospate-Buffered Saline

PCM Paracetamol

RE Reference Electrode

S Sensitivity

SEM Scanning Electron Microscope

SPE Screen-Printed Electrode

SWV Squarewave Voltammetry

WE Working Electrode

Chapter 1

Introduction

1.1 Sensors and Electrochemical Sensors

A sensor is a device capable to convert physical or chemical quantities into a signal that is detectable and analyzable [1]. Chemical sensors have the capability to detect chemical quantities, such as the concentration of an analyte in a solution [2]. The main components of a sensor are the recognition system and the transducer. The recognition system is the sensing element of the device, which interacts with the target molecule changing its properties [3]. Instead, the transducer converts the signal generated by the interaction between the analyte and the sensitive element into a measurable signal [1]. According to the type of physical quantity to be measured, the transducer can be electrochemical, optical, piezoelectric or thermal. Additionally, a signal processing system enables the analysis and visualization of the signal on a screen [1] (Figure 1.1).

Among various transducer types, the electrochemical type is the most commonly used [4]. An electrochemical sensor is a device which exploits a transducer capable of converting chemical information into an electrical signal as a result of the chemical interaction between the analyte and the sensor. At the sensor-electrolyte solution interface, electrochemical reactions occur between the analyte and the sensing element, resulting in an electrochemical signal [2], [3], [4].
Based on the reaction between the analyte and the sensor, a specific electrical parameter can be studied which constitutes the sensor's sensing technique. As a result, electrochemical sensors can be classified into three categories based on the signal provided:

- potentiometric sensors, where a change in potential difference between the electrodes is recorded when no current is flowing in the cell;

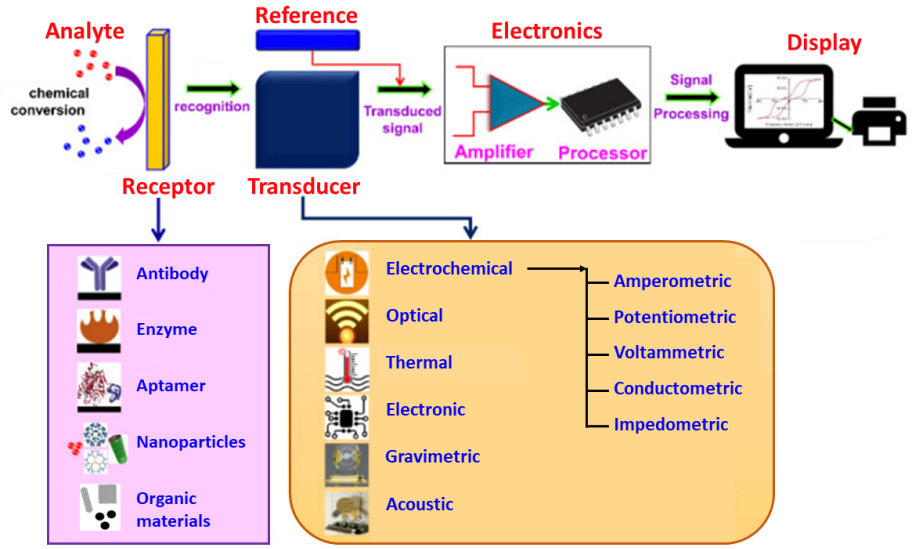

Figure 1.1: Schematic diagram of a sensor. The components are receptor, transducer, electronic system, and display. Adapted and reprinted from [2].

- amperometric sensors, for which a change in current is measured when a certain potential difference is applied;
- conductometric sensors, where a change in the conductive properties of the material between the electrodes is recorded [5].

For an amperometric sensor typically a fixed voltage is applied. However, it can also employ a time-varying voltage, and in this case, these sensors are referred to as voltammetric sensors [5].
By applying a potential, redox reactions occur at the electrode-electrolyte solution interface, causing a transfer of electrons to or from the analyte. This electron transfer is proportional to the concentration of the analyte in the solution. Consequently, in the case of this specific sensor type, the current flow is recorded in order to estimate the concentration of the target molecule [1], [4], [6].

All electrochemical sensors are extensively used due to their advantageous properties compared to other conventional analysis methods. These alternative methods, such as mass spectroscopy and fluorimetry, typically require adequately trained personnel, more expensive equipment, and longer analysis times. On the other hand, electrochemical sensors boast appealing features, including high sensitivity and selectivity, rapid response [7], cost-effective detection equipment [1], user-friendliness, and ease of miniaturization [8]. Moreover, electrochemical sensors can be easily modified while maintaining their low cost [9]. Electrochemical sensors find applications in various fields, including medical, clinical, food, and environmental

monitoring [5].

With the development of screen-printed technology, the use of Screen-Printed Electrodes (SPEs) as electrochemical sensors has gained widespread popularity.
A SPE is an electrochemical device made of multiple electrodes fabricated through screen-printing process. Specifically, these electrodes are constructed using conductive carbon or noble metals inks on a glassy or ceramic substrate [10].
SPEs commonly consist of an electrochemical cell with three electrodes: the working electrode (WE), counter or auxiliary electrode (CE) and reference electrode (RE), as shown in Figure 1.2. This arrangement is referred to as the three-electrode cell configuration [6].
By applying a potential between the working and the reference electrodes, redox reactions can occur on the working electrode depending on the applied potential's value. The redox reactions generate a flow of electrons between the working and the counter electrodes, which is recorded over time.

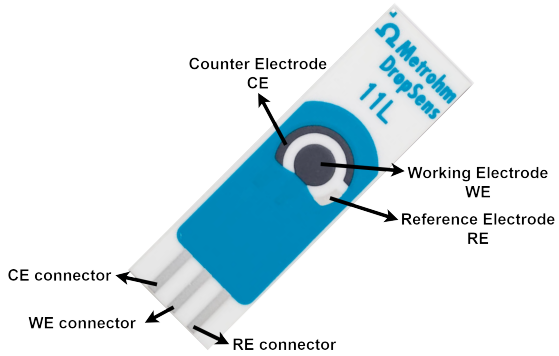

Figure 1.2: Metrohm DropSens Screen-Printed Electrode (11L) with working and counter carbon electrode, and reference electrode made of Ag/AgCl.

SPEs are miniaturised and portable sensors, characterised by their low-cost, simple and reproducible large-scale manufacturing process, user-friendliness, high sensitivity, and the capability for on-site analysis. Consequently, these sensors are disposable and feature small dimensions, allowing the use of smaller sample volumes while maintaining a low limit of detection up to picomoles [1], [8], [11]. These sensors find applications across a wide spectrum of analyses, including clinical, industrial, environmental, and agricultural domains [4]. SPEs exhibit the capability to detect both organic molecules, such as DNA [12], benzoquinone [13], and epinephrine [14], and inorganic analytes, such as Cu [15], and Hg [15].

The choice of the material and the composition of the ink, as well as the surface characteristics of the working electrode, depend on the specific sensing analysis to be conducted since these choices significantly impact the electrochemical sensor's

performance [8], [16]. Bare SPEs, typically made of carbon or gold electrodes due to their advantageous characteristics like good electron transfer kinetics, a versatile potential window, low cost, and biocompatibility, prove inadequate when the target molecule is present in small amounts in the sample, lacking sufficient selectivity [17], [18].
A notable advantage of screen-printing technology is its capability to easily modify SPEs, enhancing their performance.

Sensitivity and specificity are two pivotal characteristics of a sensor.
Sensitivity (S) for a target species is defined as the slope of the calibration curve of the system [19]. Highly sensitive sensor can detect even small change in the concentration of the species with a high response [5]. This feature is linked to the limit of detection (LoD), which represents the lowest measurable concentration, distinguishing the analyte signal from background noise [5].
An ideal sensor exhibits high sensitivity and low limit of detection, and these parameters must be reasonable for the application in which the sensor is used.
Instead, the specificity of a sensor is defined as its ability to distinguish the target analyte from other species, often referred to as interfering species, present in the sample [5].

To enhance the performance of electrodes the surface area of the working electrode can be modified. Indeed, over the last decades, researchers have increasingly integrated electrochemical sensors with biotechnology and nanotechnology to optimize them for specific applications, enhancing their performance [5]. Organic or inorganic materials can be directly incorporated into the ink composition of the SPE during the electrode manufacturing process or deposited later on the electrode surface. The functionalization of electrodes with biological, organic, and/or inorganic materials catalyzes electrolytic reactions, enhances the device's conductivity, and makes electron transfer more efficient, resulting in an enhancement of sensors' features [19].
The sensor's specificity can be heightened by modifying SPE surface with enzymes or antibodies. These biomolecules are able to catalyze specific chemical reactions, excluding interactions with interfering species [5]. Similarly, employing organic or inorganic materials like carbon nanotubes or metal/metal oxide nanoparticles increases the sensor's sensitivity by increasing the electrode surface area and enhancing the device's conductivity [5].
An overview of various examples of SPEs functionalization with biomolecules, organic or inorganic materials is provided in Figure 1.3.

Biosensors are a subset of chemical sensors wherein the receptor is a biological molecule such as enzymes, antibodies, or receptors. The biomolecule interacts with the analyte, and the transducer translates biochemical information into a measurable electrical signal [20]. Biosensors are characterised by high selectivity

and sensitivity, ease of use, and applicability for real-time and on-site analysis. Consequently, they have a very wide range of applications, including medical diagnostics, genetics, environmental monitoring, and food processes [21].

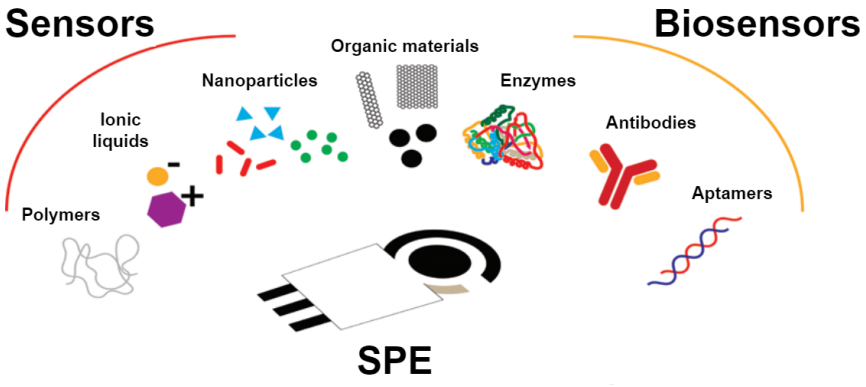

Figure 1.3: Biomolecules, organic or inorganic materials: examples of materials for the functionalization of screen-printed electrodes.

1.2 Biosensing of molecules

As discussed in Section 1.1, a biosensor incorporates a biological component as sensing element of the device. Biosensors can be categorized as catalytic or affinity-based, depending on their interaction with the analyte under analysis.
In catalytic biosensors, the biomolecule is an enzyme or another protein which catalyzes a specific chemical reaction. The bioreceptor and the analyte react chemically resulting in the formation of another species. The transducer measures the concentration of the product, and through a defined relationship determines the concentration of the analyte initially present in the solution.
Whereas, for affinity biosensors, the bioreceptor is an antibody, a binding protein or an aptamer. This bioreceptor binds specifically to a particular analyte, and the transducer directly measures the concentration of the analyte of interest [4].

1.2.1 Enzyme-modified biosensors

Enzyme-modified biosensors represent a prevalent category in biosensor technology due to their remarkable specificity. Indeed, these sensors result in a highly selective response as the enzymes interact with their specific substrates, catalyzing only targeted chemical reactions [16], [22]. However, it is essential to note that enzymes, despite their efficacy, present challenges related to high extraction costs, instability, and extreme sensitivity to environmental conditions [2].

Of all biosensors, glucose biosensors have been extensively studied and developed. Actually, they have a pivotal role in diagnosing diabetes and monitoring the blood glucose levels in diabetic patients. Electrochemical transducers, particularly of the amperometric type, are widely favored in glucose biosensors due to their superior performance in terms of sensitivity and reproducibility, coupled with their cost-effectiveness [23].
Enzymatic glucose biosensors commonly employ glucose oxidase (GOx) as sensing biomolecule. GOx offers high selectivity for glucose, cost-effectiveness, and greater tolerance to extreme conditions compared to other enzymes, both during the manufacturing and storage processes [16], [23].
The simplest glucose biosensor, denoted as first-generation sensor (Figure 1.4 (a)), utilizes GOx complexed with Flavin Adenine Dinucleotide (FAD). In this configuration, glucose undergoes oxidation to gluconic acid, simultaneously reducing the GOx-FAD$^+$ complex. The reduced complex is then oxidized through its reaction with oxygen, producing hydrogen peroxide. The concentration of glucose is determined by amperometrically measuring oxygen consumption, as the two are proportional, but a high potential is needed to improve the selectivity [24].
Furthermore, it's important to note that this sensor's reliability is compromised due to variations in oxygen concentration among different individuals and at different measurement sites within the body [25].

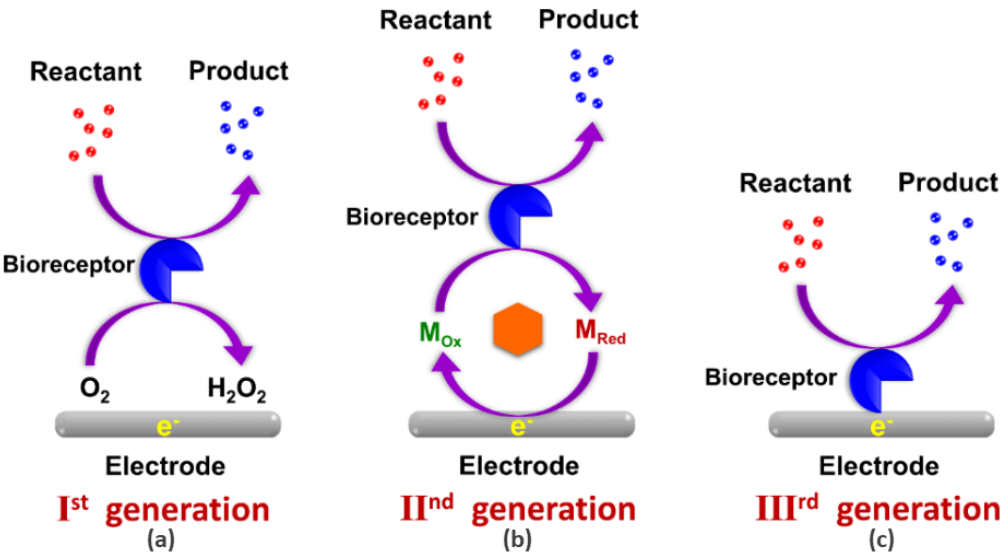

Figure 1.4: Development and improvement of enzyme-modified biosensors. In figure sensors of (a) first-generation, (b) second-generation, and (c) third-generation are shown. Used with permission from [2].

These sensors were subsequently improved through the incorporation of electronic mediators, which directly transport electrons from the enzyme to the working electrode surface [24]. This enhancement aims to directly measure glucose concentration, marking the evolution into what are commonly referred to as second-generation sensors (Figure 1.4 (b)). However, it's crucial to note that the mediator employed is a toxic and very expensive element [25].

A subsequent advancement in sensor technology led to the development of third-generation sensors (Figure 1.4 (c)). In these sensors, electron transfer occurs directly between the enzyme and the WE surface, facilitated by the attachment of GOx to nanomaterials on the working electrode [26]. This design results in improved selectivity, as glucose concentration can be directly measured without the need for any mediator [24].

Despite the continual developments and improvements in enzymatic sensors for blood glucose detection, these sensors still have limitations attributed to the utilization of GOx. This enzyme, like all enzymes, exhibits low electron transfer, its activity depends on oxygen concentration, and it is susceptible to denaturation under variations in temperature, pH, and humidity. Moreover, the construction process of these sensors is both expensive and time-consuming, as the enzyme must be immobilised on the electrode using tedious techniques [26], [27].
All these factors limit the overall performance of enzymatic sensors. Consequently, exploring the development of non-enzymatic sensors emerges as a promising solution to overcome these limitations and achieve better performance [26].

1.2.2 Immunosensors and Aptamer-based biosensors

The electrode surface can be further modified by immobilizing other biomolecules, such as antibodies. Antibodies, being proteins, selectively and specifically bind with the target antigen through affinity interactions. Sensors employing this approach are called immunosensors.
The successful interaction between the antibody and antigen can be detected by assessing physical changes resulting from complex formation or by evaluating a label attached to the antigen, which is usually a fluorescent particle, detectable through the fluorophore [2]. Immunosensors find application in various fields, including medical diagnostics, food safety, and environmental monitoring.
Within the biomedical context, immunosensors play a pivotal role in the early diagnosis of cancer by allowing the detection of tumor biomarkers present in human blood and serum. The effectiveness of these sensors is contingent upon their high sensitivity, considering that tumor biomarkers are present in very low concentrations during the early stages of cancer [28], [29].

Aptamer-based biosensors represent another prominent category of biosensors. Aptamers, defined as "synthetic single-stranded nucleic acids that selectively bind to target molecules" [2], can be immobilized on the electrode surface. The successful interaction between the aptamer and the target biomolecule can be verified using methods similar to those employed for antibody-based sensors. Aptamers exhibit remarkable versatility, as they can be chemically modified to precisely match the target molecule to be detected. Moreover, contrary to enzymes and antibodies, aptamers display stability over a wide range of temperatures and pH levels. These sensors find application in the identification of tumor cells, bacterial spores, and proteins [2].

Despite the high specificity of biosensors for the targeted analyte, they have various limitations, including the instability of the recognition element when external conditions, such as temperature and pH, changes. Moreover, a considerable number of biosensors are designed for single-use, rendering them costly [30]. Considering these aspects, this study focuses on sensors incorporating non-biomolecular recognition elements.

1.3 Sensing of molecules

As discussed in Section 1.1, the chemical modification of electrode surfaces using non-biomolecular materials has been explored to enhance the sensing features of electrochemical sensors.

In recent years, nanomaterials (NMs) have gained wide attention and application in various fields, particularly in the functionalization of electrochemical sensors. Nanomaterials exhibit different and better characteristics compared to their bulk counterparts thanks to their nanometric dimensions. Notably, their electrical, optical, mechanical, and magnetic properties are enhanced [18].
The functionalization of electrode surfaces with modifiers induces changes in the physicochemical properties of the surface, as the characteristics of the modifier are transferred to the electrode [4]. Sensors modified with NMs demonstrate improved analytical performance compared to bare sensors. This enhancement is attributed to the unique features of nanomaterials, including a higher surface-to-volume ratio, elevated electrical conductivity, efficient catalytic activity, and an enhanced electron transfer rate resulting from quantum effects [5]. The use of NMs as electroactive sensor layers extends the active surface area of the electrode, amplifies signals through catalytic activity, and facilitates chemical interactions between the analyte and the sensor's sensing unit. The sensor performance is enhanced, with improved sensitivity, reduced limit of detection, extended linearity range, and shorter analysis response time [17], [31].

Size, structure and composition of the nanomaterials involved in the electrode functionalization influence the catalytic activity and reactivity of the NM itself, and consequently the kinetics of the redox reaction between the analyte and the electrode [17], [32]. Indeed, different compositions and geometries of nanomaterials have been extensively studied to modify the surface of non-enzymatic electrochemical sensors and act as transduction elements. Inorganic nanomaterials, including metallic or metal oxide nanoparticles (NPs) and ferrocyanide, along with organic nanomaterials such as carbon nanotubes (CNTs), graphene (Gr), conducting polymers, and quantum dots, have found widespread adoption and integration into electrochemical sensors to enhance their performance. Hybrid nanomaterials, combining organic and inorganic components, have also been employed, resulting in modified sensors that exhibit either the properties of the individual constituents or novel features arising from the synergy between the materials [17], [32].

Among the various nanomaterials, ferrites have recently been a focus of extensive investigation as electrode modifiers for electrode functionalization due to the significant enhancements achievable through their utilization.

1.3.1 Ferrites nanoparticles

Spinel ferrites are complex metal oxides represented by the general formula MFe_2O_4, where M represents one or more bivalent metal cations such as Ni, Cu, Co, Zn, Fe. These ferrites exhibit a cubic crystal lattice composed of 64 tetrahedral and 32 octahedral interstitial sites (Figure 1.5 (a)). The structure of spinel ferrites can be categorized as normal, inverse or mixed, depending on how the sites are occupied:

- **Normal spinel ferrites**: bivalent ions occupy tetrahedral sites, while trivalent ions reside in octahedral sites. An example is $ZnFe_2O_4$ (Figure 1.5 (b)).
- **Inverse spinel ferrites**: bivalent cations and half of the trivalent cations occupy tetrahedral sites, while the remaining half of trivalent cations are situated in octahedral sites. An example is $CuFe_2O_4$ (Figure 1.5 (c)).
- **Mixed spinel ferrites**: bivalent and trivalent cations randomly occupy both tetrahedral and octahedral sites.

The resulting type of spinel ferrites is contingent upon factors such as the radii and charges of the cations, lattice energy, and electrostatic forces [33].

At the nanoscale, spinel ferrites exhibit superparamagnetic behavior, excellent electrocatalytic properties, chemical and thermal stability, high electrical conductivity, and a large surface area [35]. Due to these interesting characteristics, ferrites are promising in various applications within the biomedical, environmental, and

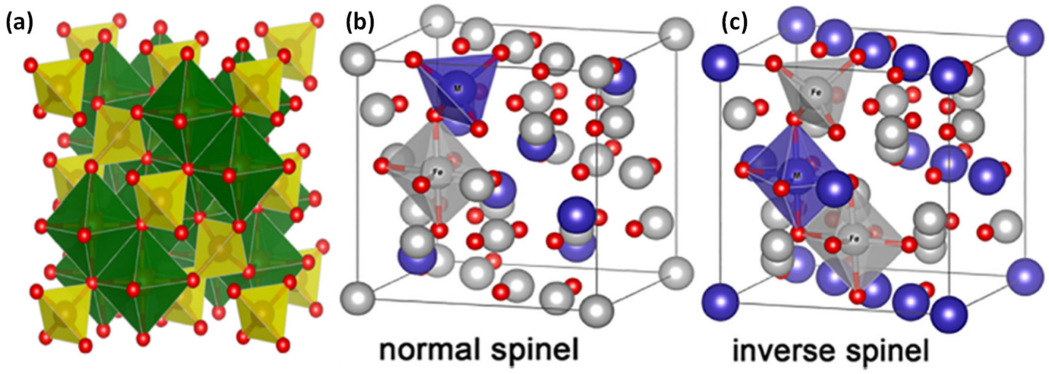

Figure 1.5: Spinel ferrites. (a) Structure of spinel ferrite with tetrahedral sites in yellow, octahedral sites in green and oxygen atoms in red. (b) Normal spinel ferrite structure. (c) Inverse spinel ferrite structure. Reprinted from [34].

industrial sectors, including areas such as energy storage, computer components, sensors, and biosensors.
The utilization of ferrites in sensing domain, particularly in electrochemical sensing area, represents a rapidly expanding field of investigation. Ferrite nanoparticles as electroactive sensor layers play a pivotal role in detecting various analytes at trace levels, demonstrating promising performance. Their utilization increases the number of active sites and enhances electrocatalytic properties, thereby improving the sensitivity, selectivity, and limit of detection of electrochemical sensors. Ferrite nanoparticles lead to a high signal-to-noise ratio, a shorter analysis times, and a reduced redox potential required for redox reactions at the electrode-analyte interface [35], [36].

1.3.2 Ferrites nanoparticles synthesis

Several methodologies are available for the synthesis of ferrites, which can be categorized into top-down or bottom-up approaches. In the former, precursor materials are decomposed to obtain nanoscale materials, while the latter involves the assembly of materials to obtain nanomaterials.

The autocombustion method is a widely employed approach for ferrite production due to it is a user-friendly, cost-effective, and fast technique [37]. This method involves a rapid exothermic chemical reaction between metal precursors (such as nitrates) and an organic fuel (such as urea). The characteristics of the resulting ferrite nanoparticles depending on the type of fuel and the ratio between fuel and precursor. This synthesis technique finds extensive application in the production of ceramic materials, composites, and ferrimagnetic nanomaterials. Its advantages include high efficiency, quick preparation, affordable cost, ease of use, and precise

control over the composition and size of the nanoparticles. It requires elevated combustion temperatures [38].

Table 1.1 outlines other main ferrite synthesis methods, providing a comparison of their respective advantages and drawbacks.

Method	**Advantages**	**Disadvantages**
Hydrothermal [39]	High crystallinity Ultra-fine material Environmentally friendly	Extreme experimental conditions
Co-precipitation [40]	Low cost Homogeneity High purity	Possible presence of impurities Reaction process time
Sol-gel [41]	Ultra-fine particles Homogeneous particles Control of parameters such as size	High cost Toxic reagents
Template [42]	Control of the nanomaterial growth	Experimental conditions regarding the template
Electrospinning [43]	Particles with high porosity and large surface area Environmentally friendly	Toxic reagents Number of parameters that must be controlled

Table 1.1: Other most widely employed ferrite synthesis methods with their respective advantages and disadvantages. Reprinted from [35].

The selection of the synthesis process significantly impacts the size and morphology of ferrite nanoparticles, thereby influencing the physical-chemical properties, sensing capabilities, and overall performance of modified sensors [35], [36]. Specifically, the size and porosity of the particles play a crucial role in determining the active surface area, thereby affecting sensor sensitivity and selectivity. Moreover, the morphology of the nanoparticles composing the electroactive layer of the sensor directly affects the interaction between the analyte and the electrode surface [35].

1.4 Paracetamol Sensing

Paracetamol (PCM), also known as acetaminophen or N-acetyl-para-aminophenol, is the most commonly used analgesic and antipyretic drug worldwide (Figure 1.6). It is prescribed to alleviate fever and provide relief from mild to moderate pain

associated with conditions such as headaches, colds, migraines, and chronic pain [44]. Moreover, PCM is used instead of aspirin or ibuprofen for patients who cannot tolerate the latter [45].

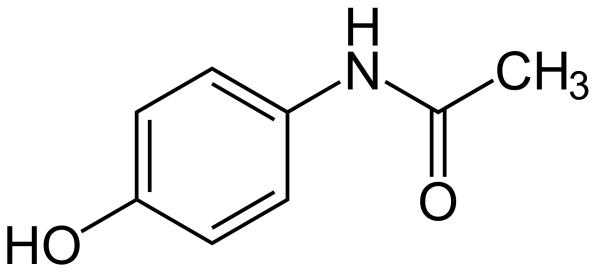

Figure 1.6: Chemical formula of paracetamol.

Paracetamol is generally well-tolerated, easily metabolized, and free from serious side effects within recommended doses. Excessive consumption of PCM can result in the accumulation of toxic metabolites, causing damage to the liver and kidneys, including acute liver necrosis, renal failure, and, in extreme cases, fatality [31], [44]. It is essential to safeguard human health by monitoring the amount of PCM present in biological fluids. PCM, like other drugs, can have environmental impacts if it is improperly disposed of, so tracking PCM in water sources to safeguard ecological health is also crucial [46]. Consequently, the development of a detection technique for paracetamol that is highly sensitive, reliable, simple, and rapid becomes essential to address both human health and environmental concerns.

Various techniques, such as spectrophotometry, chemiluminescence, capillary electrophoresis, and enzyme-based methods, have been employed for PCM sensing. However, these methods are often expensive, tedious, lack portability, and entail long analysis times, often requiring trained personnel.
Electrochemical sensing emerges as a cost-effective and highly sensitive technique which permits rapid paracetamol detection. Electrochemical sensors are user-friendly and can be easily miniaturized, enabling Point-of-Care analysis [45]. Moreover, paracetamol is electrochemically active, so electrochemical sensors are suitable for PCM detection.
Literature review reveals the increasing use of nanomaterials for electrode surface modification to detect biomolecules and drugs. Specifically, for paracetamol sensing Carbon Paste Electrodes (CPEs), Screen-Printed Carbon Electrodes (SPEs), and Glassy Carbon Electrodes (GCEs) have been utilized as electrodes. Both carbon and non-carbon nanomaterials have been explored for electrode surface modification. Some examples of modified electrodes for PCM sensing are reported in Table 1.2.

WE	Material	Method	Linearity (µM)	LoD (µM)	Ref.
CPE	Fe_2O_3	DPV	2-150	1.16	[47]
CPE	$Au@Fe_3O_4$	DPV	0.1-70	0.045	[47]
SPE	Bi_2O_2	DPV	0.5-1250	0.03	[47]
CPE	$ZnFe_2O_4$	DPV	6.5-135	0.4	[47]
CPE	ZnS	DPV	1-15	0.041	[47]
CPE	ZSM-5/TiO_2	DPV	2.5-110	0.58	[47]
GCE	VFe_2O_4	CV	0.05-12.3	0.0082	[31]
-	$CoFe_2O_4$/GP	CV	3-200	0.25	[48]
-	$MnFe_2O_4$/GP	CV	3-160	0.3	[48]
CPE	MWCNTs	SWV	2-400	0.8	[47]
CPE	Gr	SWV	2.5-143	0.6	[47]
GCE	MWCNTs	DPV	39.4-146.3	2.1	[47]
GCE	MWCNTs	SWV	0.0002-15	0.00009	[47]
GCE	MWCNT-COOH	DPV	3-300	0.6	[47]

Table 1.2: Literature examples of carbon and non-carbon nanomaterials modified electrodes used for paracetamol detection with their performance in terms of range of linearity and limit of detection.

1.5 Cyclophosphamide Sensing

Cyclophosphamide (CP), also known as cytophosphane, is a prominent anti-cancer and immunosuppressant drug extensively applied in the treatment of various malignancies, such as leukemia, breast cancer, and malignant lymphomas [49] (Figure 1.7).
Similar to other pharmaceuticals, CP is associated with various side effects, including common occurrences like vomiting, nausea, hair loss, and temporary reduction in blood cell production [50]. Hence, monitoring of cyclophosphamide concentration in the bloodstream is crucial.

Conventional techniques for detecting cyclophosphamide, such as titration and high-performance liquid chromatography, exhibit several limitations, such as high equipment costs, time-consuming procedures, and sensitivity and selectivity deficits. Electrochemical sensors are a promising alternative for cyclophosphamide detection, even if CP does not show an electrochemical behavior on its own.

An electrochemical method for CP sensing involves the utilization of amperometric

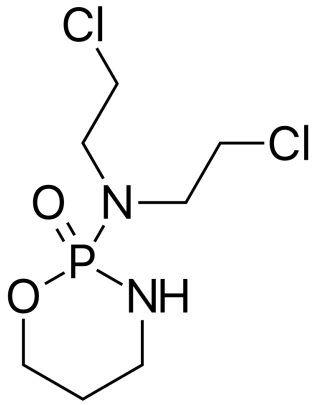

Figure 1.7: Chemical formula of cyclophosphamide.

biosensors which employ cytochrome P450 (CYP450). This enzyme possesses the capability to reduce and oxidize a wide range of endogenous and exogenous substances, including drugs like cyclophosphamide.
Among the biosensors commonly employed, the second- and third-generation biosensors, which use a mediator and are mediatorless, respectively, stand out. Mediatorless sensors are preferred, as the mediator may also promote additional redox reactions beyond those occurring between the electrode and the enzyme, leading to a decrease in selectivity.
A critical determinant of electrode performance is the proper adhesion of the enzyme to the electrode surface. Precise positioning for optimal electron transfer and preventing protein denaturation is crucial to avoid the formation of insulating layers which impede electron transfer [51]. Enhancing the adhesion of CYP can be achieved through various methods, one of which involves the use of nanomaterials. Indeed, nanomaterials, such as gold nanoparticles, metal dioxides, and notably carbon nanotubes, offer advantages such as enhancing the catalytic electrochemical activity of enzymes, and enhancing the electron transfer. CNTs have been extensively studied and used due to their ability to facilitate direct electronic transfer between the enzyme's active site and the electrode.

One established method for electrochemical sensing of the cyclophosphamide is the biosensor developed by Baj-Rossi et al. [52]. In their work, they designed a biosensor specifically for cyclophosphamide detection, incorporating multi-walled carbon nanotubes and cytochrome P450. Through CV measurements conducted at a scan rate of 20 mV/s, allowing sufficient time for the enzyme to react with the analyte, the biosensors had a sensitivity of 1.0 ± 0.1 nA/(µM·mm^2) and a detection limit of 2.4 ± 0.1 µM testing CP solutions in 0.1 M PBS, with concentrations ranging from 0 to 70 µM.

1.6 Project Aim

The aim of this research is to enhance the performance of non-enzymatic electrochemical sensors in drug detection, specifically paracetamol and cyclophosphamide sensing. The focus of the thesis is on synthesising some nano-oxides, specifically zinc ferrite, cobalt ferrite, and copper ferrite, for the functionalization of the working electrode of commercially available screen-printed carbon electrodes through drop-casting.
Cyclic voltammetric measurements will evaluate the detection capabilities of the electrodes modified with synthesised ferrites for these drugs.
For paracetamol sensing, an initial kinetic analysis of the redox reactions will be conducted, evaluating the electron transfer coefficient, kinetic constant rate, and diffusion coefficient. Subsequently, calibration curves, sensitivity, and detection limit will be obtained for both the bare sensor and all the modified electrodes.
Regarding cyclophosphamide detection, the investigation will assess the feasibility of using these ferrites for cyclophosphamide sensing, concluding with the calculation of calibration curves, sensitivity, and detection limit.
The final aim is to study the feasibility of using these nano-oxides for designing electrochemical sensors, determining the material that exhibits optimal performance for detecting these drugs, thereby paving the way for further applications in the field of sensing and biosensing.

Chapter 2

Theoretical Background

2.1 Theory of Electrochemistry

Electrochemistry is a branch of chemistry dedicated to investigating phenomena resulting from the concurrent interaction of chemical and electrical effects. This field studies the chemical processes which drive the movement of electrons.

A pivotal electrochemical concept is the redox reaction, wherein an exchange of electrons occurs between two entities identified as donor (D) and acceptor (A). In this process, electrons migrate from the donor to the acceptor, leading to the oxidation of the former and the reduction of the latter (equation 2.1). This electron transfer results in the production of a measurable electric current.

$$D + A \longrightarrow D^+ + A^- \tag{2.1}$$

Redox reactions can occur between two molecules or involve a species interacting with an electrode, denoted as homogeneous electron transfer and heterogeneous electron transfer, respectively.
Homogeneous electron transfer occurs from the highest occupied molecular orbital (HOMO) of the donor to the lowest unoccupied molecular orbital (LUMO) of the acceptor, driven by the higher energy level of the LUMO compared to the HOMO (Figure 2.1 (a)).
Similarly, in heterogeneous transfer, the electron moves from the electrode to the LUMO of the molecule, driven by the lower energy possessed by the electron present in the LUMO compared to the energy of the electrons in the electrode (Figure 2.1 (b)). The manipulation of the energy level of the electrons in the electrode can be easily achieved using a potentiostat. Indeed, the application of voltage to the electrode induces changes in electrons energy levels, creating favourable conditions for facilitating electron transfer.
In both homogeneous and heterogeneous electron transfer, the disparity in energy

levels between the orbital levels or between the electrode and the LUMO determines the electron transfer.
The present study will focus on heterogeneous electron transfer, as it explores redox reactions between an electrode and chemical species.

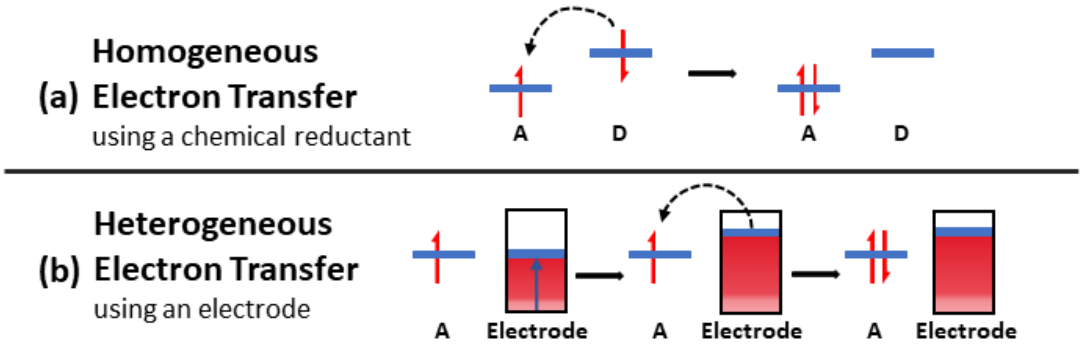

Figure 2.1: Homogeneous (a) and heterogeneous (b) electron transfer. A is the acceptor and D is the donator. The energy level of the electrons in the electrode is controllable with a potentiostat.

2.1.1 Nernst Equation

The Nernst equation describes the equilibrium between the reduced and oxidized species in a redox reaction .The Nernst equation is expressed by equation 2.2

$$E = E^0 + \frac{RT}{nF} ln\left(\frac{(Ox)}{(Red)}\right), \tag{2.2}$$

where E represents the electrochemical cell potential, E^0 the species standard potential, (Ox) and (Red) the activities of the oxidized and reduced analyte, F the Faraday constant, R the universal gas constant, T the temperature, and n the number of electrons involved in the redox reaction.
The concentrations of the oxidized and reduced species (c_O, c_R) typically replace their respective activities as they are more easily determined experimentally. Indeed, the formal potential E'^0 is usually utilized in place of E^0, since E'^0 is specific to experimental conditions and is frequently estimated as the average potential between reduction potential and oxidation potential, denoted as $E_{1/2}$. Based on the concentration of the oxidized or reduced species, or based on the potential applied to the cell, via equation 2.3, the behavior of the system can be predicted [53].

$$E = E'^0 + \frac{RT}{nF} ln\left(\frac{c_O}{c_R}\right) \tag{2.3}$$

2.1.2 Electrode Reactions

An electrode reaction involves the transfer of one or more electrons between the electrode and the analyte at the electrode/electrolyte solution interface. In the reduction of a species O (equation 2.4), the process includes the transport of the reactant O to the electrode surface, the transfer of electrons from the electrode to the reactant, the occurrence of the reduction reaction, and ultimately, the removal of the reduced species R from the interface.

$$\mathrm{O} + \mathrm{ne}^- \longrightarrow \mathrm{R} \tag{2.4}$$

The progression of these steps, and consequently, the kinetics of the redox reaction, depend on multiple factors, including the applied potential to the electrode, the specific species undergoing reduction, and the electrode surface.

2.1.3 Redox Reaction Kinetics

The redox reaction kinetics, and consequently, the resulting current, depend on two key factors:

1. kinetics of the electron transfer between the electrode and the analyte;
2. kinetics of the transport of species O to the electrode and species R from the electrode.

Considering a redox reaction involving a single electron transfer (equation 2.5)

$$\mathrm{O} + \mathrm{e}^- \underset{\mathrm{k_{ox}}}{\overset{\mathrm{k_{red}}}{\rightleftharpoons}} \mathrm{R}, \tag{2.5}$$

the anodic current i_a and the cathodic current i_c result to be:

$$i_a = -F \cdot A \cdot k_{red} \cdot \bar{c_o} \tag{2.6}$$

$$i_c = F \cdot A \cdot k_{red} \cdot \bar{c_r}. \tag{2.7}$$

These currents depend on the electrode area (A), the species concentration on the electrode surface ($\bar{c_r}, \bar{c_o}$), the electron transfer rate (k_{red}), and Faraday constant (F). By convention, the cathodic current is positive, and the anodic current is negative.

2.1.4 Mass Transport Kinetics

The rate at which the analyte is transported to the electrode significantly impacts the kinetics of the overall redox reaction.

Referring to equation 2.7, the cathodic current i_c depends on the kinetics of electron transfer (k_{red}), as well as the concentration of the reagent on the electrode surface ($\bar{c_r}$). Focusing only on the contribution of the concentration of the reactant species, various modes of solute movement in the solution can occur. Indeed, so-called mass transport can occur through:

1. diffusion, induced by a concentration gradient;
2. migration, resulting from an electric potential gradient;
3. convection, driven by temperature, pressure or density gradients, and forced agitation.

The experimental conditions used in this study permit the simplification of the theory of mass transport.
Firstly, mass transport via convection can be excluded by avoiding agitation.
Furthermore, the migration-driven transport of the analyte can also be neglected by introducing an inert support electrolyte with a much higher concentration than the species under analysis and electrochemically inert in the considered potential range. The use of this support electrolyte also enhances the solution's conductivity.
In conclusion, given these considerations, it can be deduced that the analyte is predominantly transported through diffusion.

2.1.5 Diffusion Mass Transport - Fick's Laws

In absence of redox reactions, the species' concentration profile is homogeneous throughout the entire solution, from the electrode surface to the bulk solution.
However, during redox reactions, which occur at the electrode-solution interface, the concentration of species at this interface becomes lower compared to bulk solution. This determines a concentration gradient of the reagent at the interface. Simultaneously, the product of the redox reaction becomes more concentrated at the interface than in the bulk solution.
The mathematical explanation for mass flow through diffusion is provided by Fick's laws.

Fick's first law in vector form is expressed by equation 2.8

$$\vec{j_m} = -D \cdot \vec{\nabla} c(\vec{x}, t), \tag{2.8}$$

stating that the diffusion flux of a species $\vec{j_m}$ is directly proportional to the concentration gradient within the solution, and has a direction determined by this gradient. In equation 2.8, D represents the diffusion coefficient of the diffusing species, influenced by the interactions between the diffusing species and the solvent molecules. The negative sign in equation 2.8 is to indicate that diffusion-driven

molecular flow occurs from high concentration to low concentration area.
Fick's first law describes the concentration flow as a function of distance, without providing the temporal evolution of the concentration.

Fick's second law (equation 2.9) describes the concentration profile as a function of both distance from the electrode surface and the electrolysis time. The diffusion velocity increases proportionally with the magnitude of the change in concentration.

$$\frac{\partial c(x,t)}{\partial t} = D \cdot \frac{\partial^2 c(x,t)}{\partial x^2} \tag{2.9}$$

2.2 Cyclic Voltammetry

An electrochemical system can be effectively studied by applying a suitable potential and analyzing the resulting current, which is directly proportional to the analyte concentration in the solution.

Voltammetry measures the current resulting from redox reactions occurring by applying a time-varying potential. This technique not only provides analytical information such as the analyte concentration, but also offers thermodynamic details concerning the redox potentials and kinetic information in terms of the reaction rates.

Cyclic voltammetry (CV) is a specific form of voltammetry widely employed for characterizing electrochemically unknown systems. In this approach, a triangular potential pattern is applied between the working electrode and the reference electrode through the utilization of a potentiostat. During the forward scan, the potential varies from E_1 to a designated switching potential E_2, and during the reverse scan, it varies from E_2 back to E_1. This cyclic reversal of the potential scan induces the reduction (or oxidation) followed by the oxidation (or reduction) of the analyte under investigation. Concurrently, the current flowing between the working and counter electrodes is recorded.
The graphical representation of potential and current obtained during the potential scan is called cyclic voltammogram. The applied voltage is depicted on the y-axis, while the current is plotted on the x-axis (Figure 2.2). According to the IUPAC convention, which has been followed in this study, the x-axis runs from negative to positive potential values [53]. Additionally, the cathodic current is depicted as negative, whereas the anodic current is represented as positive.
By modifying the applied potential through a potentiostat, in accordance with Nernst equation (equation 2.3), the concentrations of the oxidised and reduced species in the solution close to the electrode change. In Figure 2.2, two distinct current peaks are distinguishable, one associated with the oxidation process and the other with the reduction process. These peaks occur at a specific potential

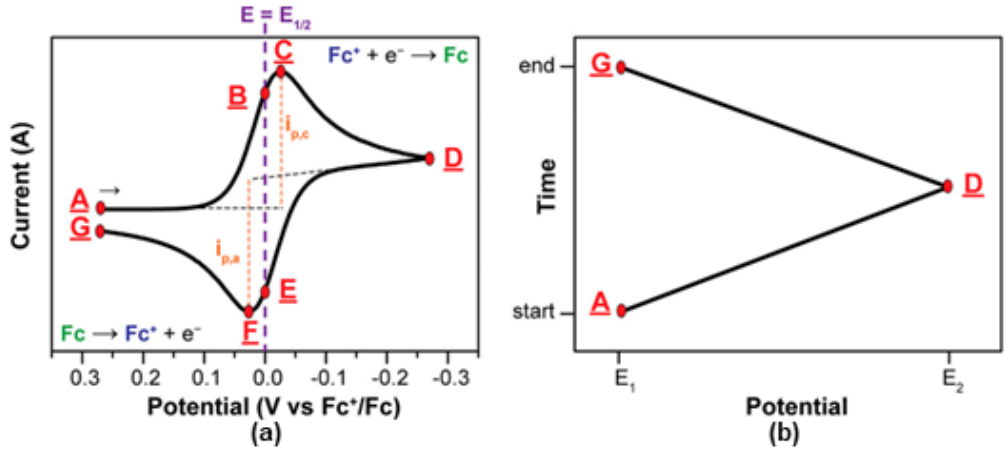

Figure 2.2: (a) Cyclic voltammetry of the reduction of Fc^+ to Fc following the US convention (the opposite of the IUPAC convention adopted in this study). (b) Evolution of the applied potential with an initial potential E_1 higher than the switching potential E_2. Reprinted from [53].

applied to the electrochemical cell. Therefore, by applying a potential with a cyclic triangular pattern, this technique induces a cyclical progression of oxidation and reduction of the species.
Cyclic voltammetry provides information about the potentials at which the redox reactions of the analyte, specifically the reduction and oxidation potentials, occur. The non-coincidence of these potentials is a consequence of the analyte's diffusion to and from the electrode.
The average potential between the two peaks provides an estimation of the formal potential $E_0^{'}$ associated with a reversible electron transfer. The difference between the oxidation and reduction potentials, denoted as ΔE_p, is called peak-to-peak separation.

2.3 Randles-Sevčik Equation

A pivotal parameter in cyclic voltammetry measurements is the scan rate ν (mV/s), indicating the rate at which the potential changes over time. Indeed, the behavior of the analyte on the WE surface depends on this parameter. Higher scan rates result in a thinner diffusion layer, consequently resulting in higher currents.
The current peak i_p depends not only on the concentration of the analyte and its diffusion coefficient, but also on the scan rate. Specifically, for reversible electron transfers with freely diffusing redox species, the Randles-Sevčik equation

is expressed by equation 2.10

$$i_p = 0.446 \cdot nFAc \cdot \sqrt{\frac{nF\nu D}{RT}}, \tag{2.10}$$

where n is the number of electrons exchanged in the redox reaction, A is the electrode's surface area, c is the analyte concentration, and D is the diffusion coefficient of the species. Thus, the Randles-Sevčik equation states a linear relation between the peak current and the square root of the scan rate. Additionally, this equation is used to determine the diffusion coefficient of the species.
However, when the analyte is not freely diffusing in the solution, but is instead adsorbed on the electrode surface, the relation between the peak current and the scan rate is linear, necessitating the use of a different equation to correlate the two parameters.

2.4 Laviron Equations

In 1967, Laviron [54] proposed equations to determine the transfer coefficient α and the electron transfer rate of an electrochemical reaction k for diffusionless systems. Given the number of electrons involved in the redox reaction, in case $n\Delta E_p$ is greater than 200 mV/s, equation 2.11 and equation 2.12 define the slopes of the graphs for the oxidation potential and reduction potential, respectively, as a function of the logarithm of the scan rate.

$$m_c = \frac{-2.3RT}{\alpha nF} \tag{2.11}$$

$$m_a = \frac{2.3RT}{(1-\alpha)nF} \tag{2.12}$$

Through the calculation of the value of these slopes, the transfer coefficient can be determined by equation 2.13.

$$\alpha = \frac{m_a - m_c}{m_a} \tag{2.13}$$

Equation 2.14 allows the calculation of the electron transfer rate with the determined value of alpha.

$$logk = \alpha log(1-\alpha) + (1-\alpha)log\alpha - log\left(\frac{RT}{nF\nu}\right) - \alpha(1-\alpha)\frac{nF\Delta E_p}{2.3RT} \tag{2.14}$$

The Laviron's work [54] demonstrates also how to determinate α and k for systems in which $n\Delta E_p$ is not greater than 200 mV.

Chapter 3

Materials and Methods

All nanomaterials exploited in this project were synthesised at the Carbon Group at Politecnico di Torino, Italy, with the help of Dr. Mattia Bartoli, following the method proposed by Madagalam et al. [37]. Electrodes functionalization and performance testing were carried out at the Bio/CMOS Interfaces group at École Polytechnique Fédérale de Lausanne, Switzerland.

3.1 Chemicals

All chemicals employed in this project were purchased from Sigma-Aldrich and utilised without any modification.
In the ferrite synthesis process, copper(II) nitrate trihydrate ($Cu(NO_3)_2 \cdot 3H_2O$), cobalt(II) nitrate hexahydrate ($Co(NO_3)_2 \cdot 6H_2O$), iron(III) nitrate heptahydrate ($Fe(NO_3)_3 \cdot 7H_2O$), zinc(II) nitrate hexahydrate ($Zn(NO_3)_2 \cdot 6H_2O$), and urea ($CO(NH_2)_2$) were used.
Butanol ($C_4H_{10}O$) was employed to obtain suspensions containing the synthesized ferrites, which were subsequently used to functionalize the electrodes. For cyclophosphamide detection, some ferrite-modified sensors underwent additional functionalization with cytochrome P450, isoform CYP3A4.
To prepare the electrolyte solutions for paracetamol and cyclophosphamide sensing, paracetamol ($C_8H_9NO_2$) and cyclophosphamide ($C_7H_{15}Cl_2N_2O_2P \cdot H_2O$) were used with Phosphate-Buffered Saline (PBS) buffer.

3.2 Ferrites nanomaterials synthesis

Ferrite nanomaterials were synthesised via the autocombustion technique. A schematic of the adopted method is shown in Figure 3.1.

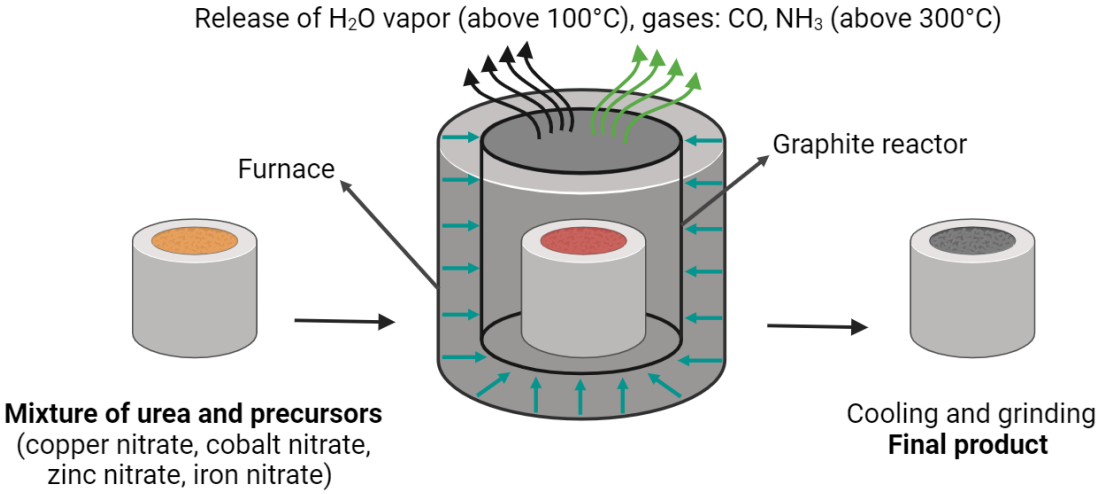

Figure 3.1: Schematic diagram of the working principle of the autocombustion technique adopted for the synthesis of ferrite nanomaterials.

The stoichiometric ratios of copper nitrate, cobalt nitrate, zinc nitrate, and iron nitrate were used as oxidizing agents, and urea was used as a reducing agent. Depending on the final compound that was to be synthesised, a mixture of materials was prepared in a crucible, using the amounts shown in Table 3.1 in order to obtain 500 mg of each final material. Adding a constant amount of urea (1 g) for each synthesis process, precursor solutions were obtained.

Material	$Co(NO_3)_2$ (g)	$Cu(NO_3)_2$ (g)	$Zn(NO_3)_2$ (g)	$Fe(NO_3)_2$ (g)
$CoFe_2O_4$	0.620	-	-	1.722
$CuFe_2O_4$	-	0.505	-	1.689
$ZnFe_2O_4$	-	-	0.617	1.676

Table 3.1: Reactants masses used for $CoFe_2O_4$, $CuFe_2O_4$, and $ZnFe_2O_4$ nanoparticles synthesis.

The crucible was placed inside a graphite reactor. Placed in a furnace, the materials were heated to a temperature of 600°C starting from room temperature, and were kept at the temperature of 600°C for 1 hour. Then, the materials were cooled in air to room temperature, and fine ferrite powders were collected. Table 3.2 shows the amount of cobalt ferrite, copper ferrite and zinc ferrite powders collected, and their respective percent yield.

Material	Actual yield (mg)	Percent yield (%)
$CoFe_2O_4$	340	68%
$CuFe_2O_4$	246	49%
$ZnFe_2O_4$	240	48%

Table 3.2: Amount of synthesized products collected with their respective percent yield.

3.3 Electrodes Functionalization

3.3.1 Functionalization with Ferrites

The sensors exploited in this study are the 11L electrodes fabricated by Dropsens, consisting of a working and counter carbon electrode, and a reference electrode made of Ag/AgCl. The working electrode's diameter is 4 mm, providing a surface area of 0.12 cm^2. An 11L SPE is shown in Figure 1.2.
The functionalization of the working electrode with the synthesised ferrites was performed by drop-casting technique, recognized as one of the simplest and most effective, and therefore widely adopted methods for the electrode surface modification [35].

Suspensions containing the ferrites were prepared to modify the electrodes. To facilitate the attainment of a homogeneous suspension, the ferrites were initially crushed through the use of a mortar. Subsequently, suspensions containing the ferrites were prepared adding 3 mg of pulverized ferrites into 1 mL of butanol, following the methodology of Madagalam et al.'s work [37]. To ensure homogeneity of the suspensions, the latter were put in an ultrasonic bath for 30 minutes. Thus, the suspensions were ready to be used for the electrode functionalization. By drop-casting technique a suspension drop of 5 µL was delicately placed on the working electrode's surface using a micropipette, followed by an overnight drying process at room temperature to evaporate the solvent and fix the ferrites on the top of the electrode surface.

3.3.2 Functionalization with Ferrites and Cytochrome P450

For the detection of cyclophosphamide, some copper ferrite-modified sensors were additionally functionalized with cytochrome. These sensors were further modified with 3 µL of a solution containing CYP3A4 using drop-casting technique. The electrodes were then stored in a refrigerator at 4°C overnight to allow the enzyme to bind to the copper ferrite.

3.4 Materials Characterization

3.4.1 Raman Spectroscopy

Raman spectroscopy is an analytical technique exploiting Raman scattering, a phenomenon occurring when light interacts with a sample, inducing a shift in its frequency, known as Raman shift. With this technique, a sample is exposed to a beam of light at a certain frequency, and, upon their interaction, part of the incident photons is scattered, changing the radiation frequency. This shift provides information about the sample, elucidating structural characteristics, electronic environment features, chemical composition and molecular bonds.

In this study, Raman spectroscopy measurements (Renishaw, inVia Raman Microscope) were performed to investigate the crystalline phase of materials. A laser excitation wavelength of 785 nm (IR light) was employed.

3.4.2 Field Emission Scanning Electron Microscopy

Field-Emission Scanning Electron Microscopy (FESEM) is an electron microscopy technique employed to probe the morphology and surface characteristics of materials at high resolution, reaching to the nanoscale.
This technique entails irradiating the sample with a focused beam of high-energy electrons, determining the emission of secondary electrons due to interaction with the sample. These emitted electrons are then collected and utilized to obtain detailed surface sample images, accessing to an examination of its morphology and topography.

In this project, FESEM analyses (Zeiss Supra 40, Oberkochen, Germany) were performed on the synthesized nanomaterials to investigate their morphology. Additionally, FESEM analyses of ferrite-modified sensors were carried out to evaluate sensors functionalization.
The energy of the electron beam was fixed at 5 keV, and images were obtained using secondary electrons.

3.5 Electrolytic Solution Preparation

3.5.1 PBS Solution

Phospate-Buffered Saline was chosen as electrolyte based on its similarity to the ion concentration and pH regulation observed in the human body. Thus, a 0.1 M PBS solution was prepared by dissolving a PBS tablet in 20 mL of deionized (DI) water. This solution has a pH of 7.4 at 25°C.

3.5.2 Paracetamol Solution

5.0 mM paracetamol solution was obtained by dissolving 35.3 mg of PCM in 46.7 mL of 0.1 M PBS solution. Paracetamol solutions with lower molarities were derived through successive dilutions, with the volume quantities of PBS and PCM solutions reported in Table 3.3. All paracetamol solutions were stored at 4°C.

final PCM molarity	5.0 mM PCM volume	0.1 M PBS volume
0.5 mM	12.0 mL	8.0 mL
1.0 mM	10.0 mL	10.0 mL
1.5 mM	8.0 mL	12.0 mL
2.0 mM	6.0 mL	14.0 mL
2.5 mM	4.0 mL	16.0 mL
3.0 mM	2.0 mL	18.0 mL

Table 3.3: Volumes of 0.1 M PBS and 5.0 mM PCM solutions used to obtain 20.0 mL of PCM solutions at the desired concentrations (from 0.5 to 3.0 mM in steps of 0.5 mM).

3.5.3 Cyclophosphamide Solution

1.0 mM cyclophosphamide solution was obtained by adding 4.3 mg of CP in 15.4 mL of 0.1 M PBS solution. Cyclophosphamide solutions with reduced concentrations were prepared by progressively diluting the original solution. The specific volume quantities of PBS and CP solutions are shown in Table 3.4. All cyclophosphamide solutions were kept at a temperature of 4°C.

final CP molarity	1.0 mM CP volume	0.1 M PBS volume
10 µM	0.05 mL	4.95 mL
50 µM	0.25 mL	4.75 mL
100 µM	0.50 mL	4.50 mL
150 µM	0.75 mL	4.25 mL
200 µM	1.00 mL	4.00 mL

Table 3.4: Volumes of 0.1 M PBS and 1.0 mM CP solutions used to obtain 5.0 mL of CP solutions at the desired concentrations (10, 50, 100, 150, and 200 µM).

3.6 Cyclic Voltammetry Measurements

The electrochemical behaviour of the two drugs has been studied by cyclic voltammetry measurements via the AUT302N.MBA.S potentiostat provided by Autolab Metrohm. The potentiostat was connected to the electrode under analysis and to a computer in order to collect and display data in real time. A scheme of the electrochemical measurement setup is presented in Figure 3.2.

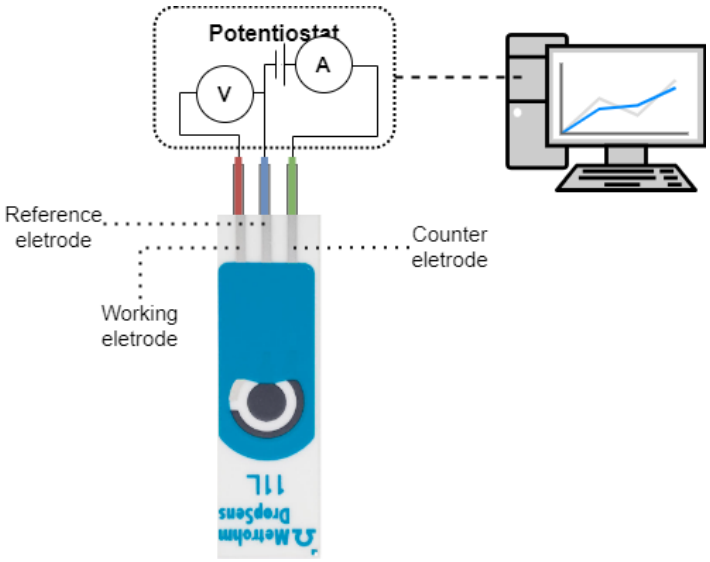

Figure 3.2: Schematic setup of the electrochemical measurement. The potentiostat is linked to both the electrochemical system and the personal computer to display and analyze cyclic voltammetry measurements.

A 100 µL drop of electrolyte solution well covered all the three electrodes of the SPE. The range potential imposed between the RE and the WE for paracetamol and cyclophosphamide detection are shown in Table 3.5.

Analyte	Upper Potential (V)	Lower potential (V)
Paracetamol	-0.6	0.8
Cyclophosphamide	-0.6	0.4

Table 3.5: Potential ranges imposed between the reference and working electrodes for paracetamol and cyclophosphamide sensing.

3.6.1 Paracetamol Sensing Measurements

Figure 3.3 shows the workflow of the measurements performed for each electrode for paracetamol sensing.

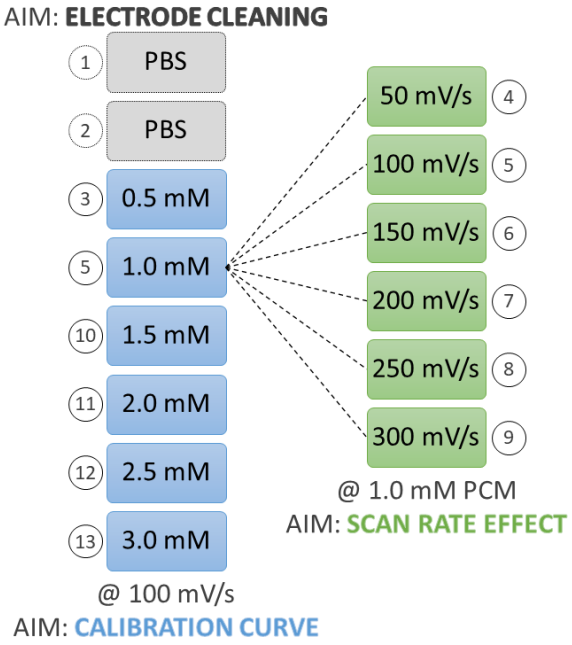

Figure 3.3: List of the conducted CV measurements for each electrode for paracetamol sensing. Parameters set for deriving the calibration curve are reported in blue, whereas parameters utilized for analyzing the effect of the scan rate are reported in green. The concentrations indicated are the concentrations of the PCM solutions, whereas the PBS solution has a fixed concentration of 0.1 M.

To clean the electrodes after the surface modification, two cleaning steps were performed, conducting CV measurements using blank solution of 0.1 M PBS (Figure 3.3, grey part) with a number of scan equal to 10. Then, CV measurements were performed with PCM solutions at increasing concentrations. Between successive CV measurements, the electrode was cleaned with a gentle flow of DI water, followed by subsequent air-drying. An overview of the PCM concentrations used and the scan rate set are shown in Figure 3.3. The number of scans for each CV measurement with PCM solutions was set to 5.
To evaluate and compare the performance of bare and modified electrodes with various materials, CV measurements were conducted using 1.0 mM PCM solution at a fixed scan rate of 100 mV/s.
To investigate the redox reactions kinetics, the PCM solution concentration was fixed to 1.0 mM, and the scan rates was varied from 50 to 300 mV/s in steps of 50

mV/s (Figure 3.3, green part).
For the calibration curve derivation, CV measurements were performed at a fixed scan rate of 100 mV/s, varying the PCM solution concentration from 0.5 to 3.0 mM in steps of 0.5 mM (Figure 3.3, blue part).

3.6.2 Cyclophosphamide Sensing Measurements

Figure 3.4 shows the workflow of the measurements performed for cyclophosphamide sensing.

Figure 3.4: List of the conducted CV measurements for cyclophosphamide detection. Parameters set for deriving the calibration curve are reported in blue. The concentrations indicated are the concentrations of the CP solutions, whereas the PBS solution has a fixed concentration of 0.1 M.

The cleaning protocol involved two cycles with 0.1 M PBS solution (Figure 3.4, grey section), with a total of 10 scans. Then, CV measurements were performed with CP solutions at increasing concentrations in order to derive the calibration curve. CV measurements were performed at a fixed scan rate of 20 or 100 mV/s, varying the CP solution concentration from 10 to 200 µM (Figure 3.4, blue part). Each CV measurement consisted of 5 scans. Between consecutive CV measurements, the CP solution drop was replaced, and the electrode underwent a cleaning process using a gentle stream of DI water, followed by air drying.

Chapter 4

Results and Discussions

4.1 Materials Characterization

4.1.1 Raman Spectroscopy

Raman spectroscopy analysis consists of exposing a sample to electromagnetic radiation and examining the resulting scattering phenomena. The Raman spectrum reveals the molecular vibrational modes of the analysed substance, which constitutes the material's fingerprint. This spectrum provides a comprehensive overview of the analyzed sample, including structural details, electronic environment characteristics, and the molecular bonds [55]. Consequently, different materials exhibit different Raman spectra, allowing them to be differentiated through visual examination of their respective spectra. Raman spectroscopy can validate the proper synthesis of materials by comparing their spectra with literature references, and this is the approach adopted in this study. To verify the identity of the synthesized materials as the targeted ferrites, a comparison was made between the Raman spectra of zinc ferrite, cobalt ferrite, and copper ferrite obtained from the literature [37], [56], [57], reported in Figure 4.1, and the spectra obtained from the corresponding synthesized materials, shown in Figure 4.2.

Ferrites crystallise in a spinel structure. The zinc and cobalt ferrites exhibit five distinctive Raman bands, a A_{1g} band, a E_g band and three T_{2g} bands. Indeed, both in Figure 4.1 and 4.2, these five peaks can be distinguished in the Raman spectra of these ferrites. Instead, cobalt ferrite shows six active Raman modes attributed to a E_g band, two A_{1g} bands, and three T_{2g} bands. Indeed, six peaks can be identified in both the Raman spectrum of the literature and that of the synthesised cobalt ferrite.
Through a detailed analysis and visual comparison of the Raman spectra, the synthesised materials correspond to the targeted ferrites.

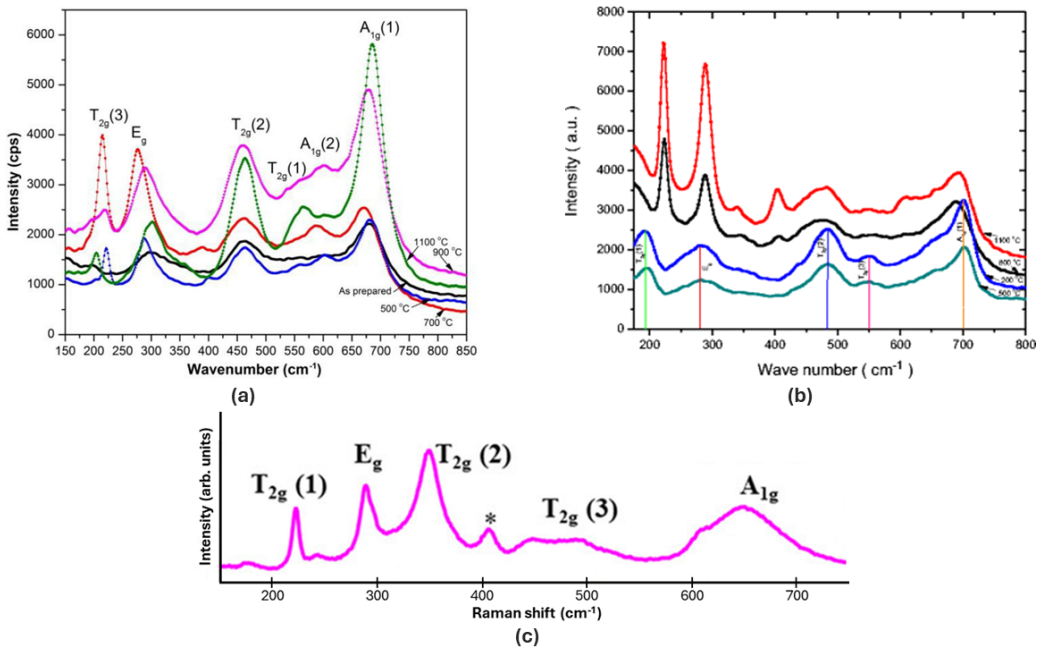

Figure 4.1: Raman spectra of (a) $CoFe_2O_4$ nanoparticles from [57], $CuFe_2O_4$ nanoparticles from [56], (c) $ZnFe_2O_4$ nanoparticles from [37] (* denotes an unknown Raman band).

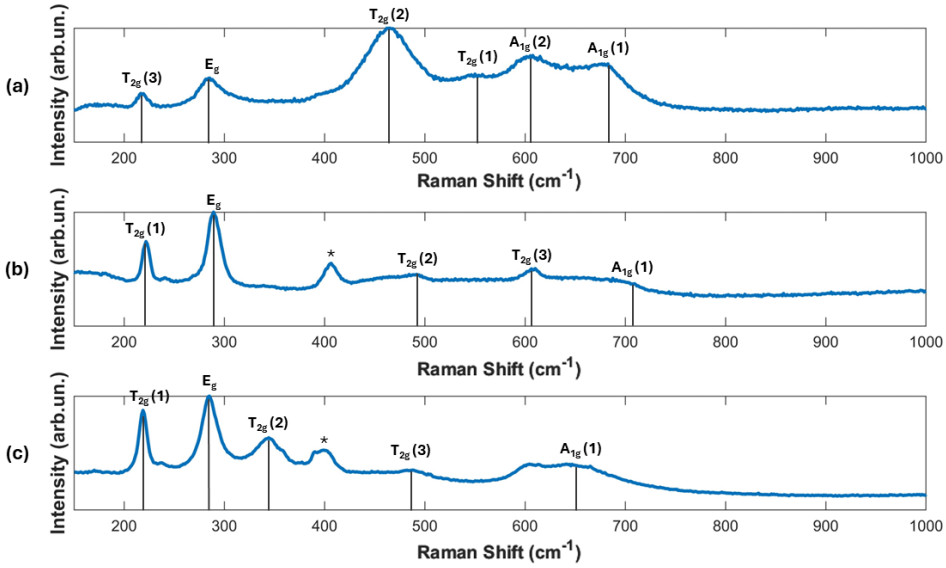

Figure 4.2: Raman spectra of (a) $CoFe_2O_4$, (b) $CuFe_2O_4$ and (c) $ZnFe_2O_4$ synthesised nanoparticles (* denotes an unknown Raman band).

4.1.2 Field Emission Scanning Electron Microscopy

To probe the morphological characteristics of the synthesised ferrites and investigate the material deposition on the working electrode surface of the SPEs, FESEM analyses were conducted for all the materials and the modified sensors. Instead, Scanning Electron Microscope (SEM) analyses were performed for the bare sensor. Both FESEM and SEM analysis allow the examination of material distribution and the morphological characteristics of the ferrites through the use of an electron beam. Notably, the electron beam employed in FESEM analysis is narrower compared to the one utilized in SEM analysis, resulting in clearer images with enhanced spatial resolution.

The bare sensor SEM images are reported in Figure 4.3, and the FESEM images of $CuFe_2O_4$, $CoFe_2O_4$, and $ZnFe_2O_4$ nanoparticles and the sensors modified with these ferrites are shown in Figure 4.4, Figure 4.5, and Figure 4.6, respectively.

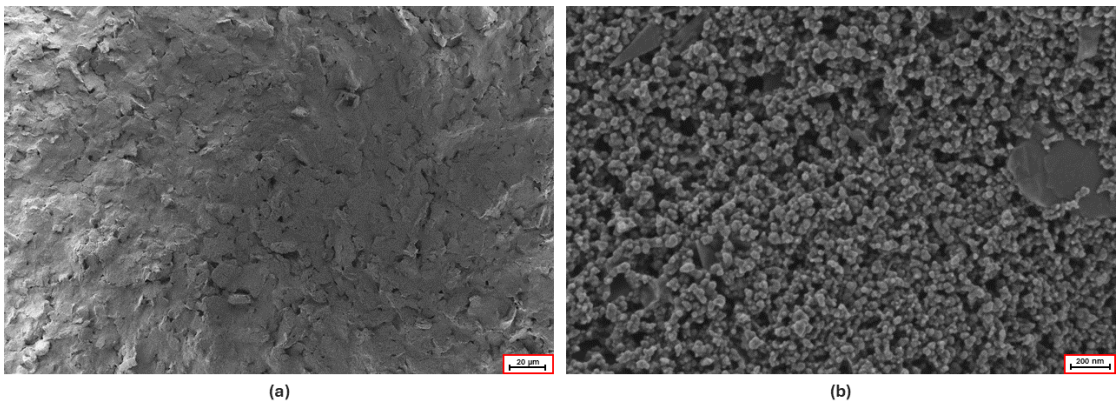

Figure 4.3: SEM analysis of bare sensor with magnification of (a) 1k x, and (b) 100k x.

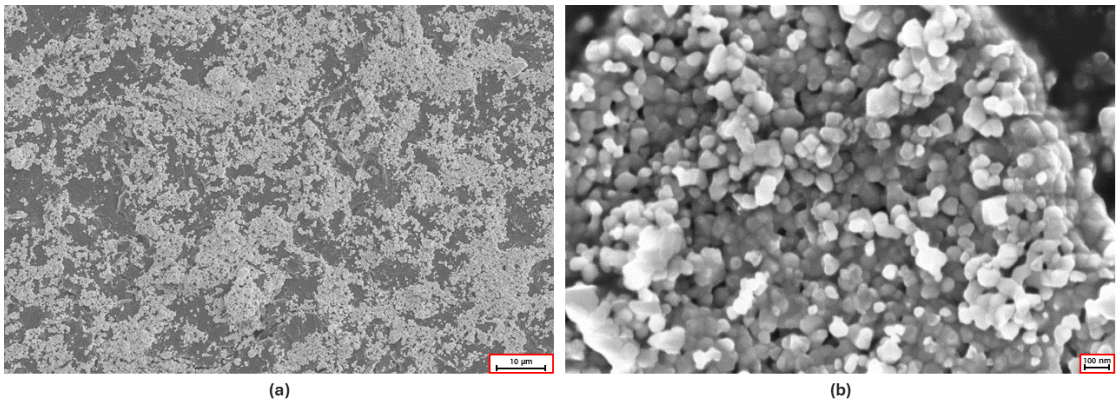

Figure 4.4: FESEM analysis of (a) $CuFe_2O_4$ modified sensor with magnification of 1k x, and (b) $CuFe_2O_4$ nanoparticles with a magnification of 25k x.

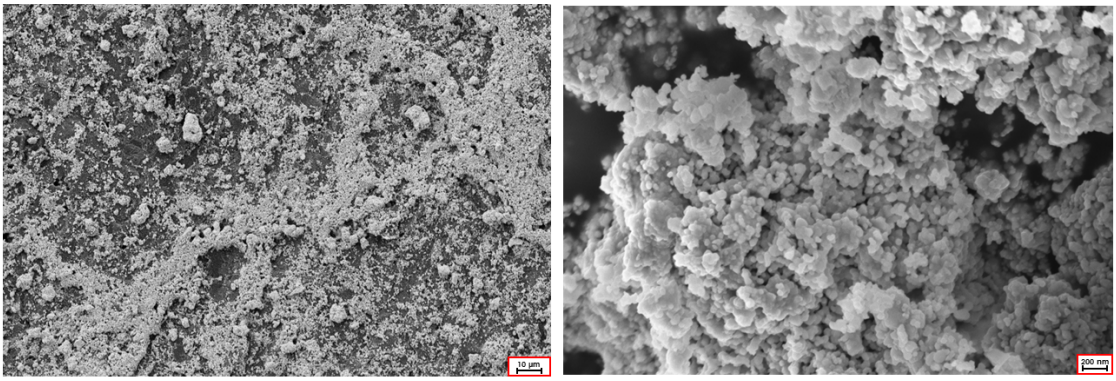

Figure 4.5: FESEM analysis of (a) $CoFe_2O_4$ modified sensor with magnification of 500 x, and (b) $CoFe_2O_4$ nanoparticles with a magnification of 25k x.

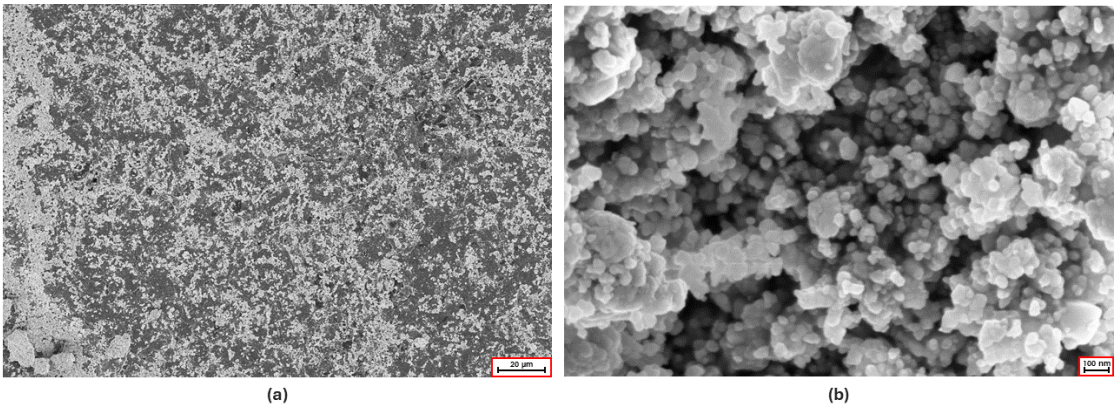

Figure 4.6: FESEM analysis of (a) $ZnFe_2O_4$ modified sensor with magnification of 500 x, and (b) $ZnFe_2O_4$ nanoparticles with a magnification of 50k x.

The material distribution on the electrode surface appears uniformly homogeneous for all the modified sensors, and there is an absence of nanoparticles agglomerates, confirming the effective dispersion of ferrites in butanol suspension.
Instead, the morphology of nanoparticles appears to be regular, with dimensions between 30 to 60 nm.

4.2 Cyclic Voltammetry - Paracetamol

Bare electrodes and electrodes modified with synthesised oxides were tested through cyclic voltammetry measurements for paracetamol sensing. As discussed in section 3.6, a drop of 100 µL of electrolyte solution was placed on the electrode surface using a micropipette in order to completely cover the three electrodes constituting the

SPE. The potential range applied to the working electrode and reference electrode was set between -0.6 V and 0.8 V vs Ag/AgCl, and simultaneously, the current flowing between the working electrode and the counter electrode was measured. For each measure conducted with a specif set of parameters in terms of scan rate and concentration of the electrolyte solution 5 scans were acquired, discarding the first two as they are unstable. Instead, the last three scans were used to calculate the average value and the standard error of the parameters of interest, taking into account intra-electrode variability. Additionally, for each material used for the electrode surface modification, 3 electrodes modified with the same material were tested in order to consider inter-electrode variability.

To investigate the electrochemical behavior of paracetamol, two cyclic voltammetry measurements were compared, one using 0.1 M PBS and the other using 1.0 mM PCM in 0.1 M PBS as electrolyte solution. In Figure 4.7, these two CV measurements are compared in the case of a bare sensor. When the electrolyte solution is a blank PBS solution, the recorded current between the electrodes appears consistently low in amplitude, ranging around 1 µA, with a flat pattern, as there are no electroactive species undergoing oxidation or reduction. This current is the background or non-faradaic current. When paracetamol is present in the electrolyte solution, the current flowing between the WE and CE, the so-called faradaic current, exhibits a different profile, showing distinguishable peaks of oxidation and reduction. This occurs because PCM is an electroactive species within the set potential range.

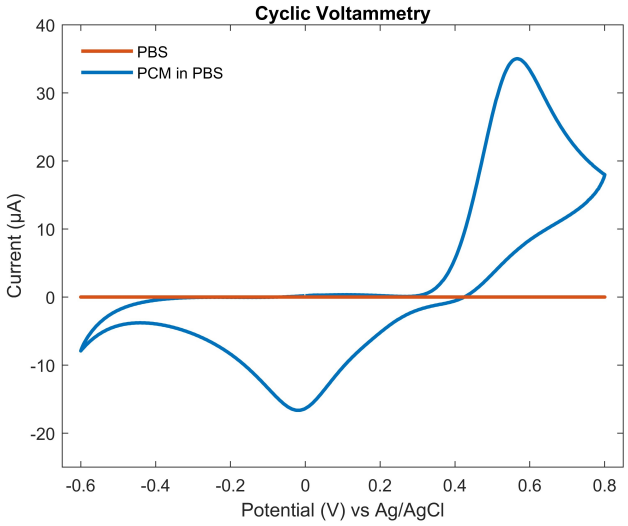

Figure 4.7: Cyclic voltammetry of a bare sensor at a fixed scan rate of 100 mV/s with 0.1 M PBS (orange) and 1.0 mM PCM in 0.1 M PBS (blue).

The current has the same behavior also in the case of modified electrodes as shown in Figure 4.8 for the zinc ferrite sensor. Specifically, in the case of modified sensors, the current obtained during the CV measurement with only PBS is less flat compared to the signal obtained with the bare sensor, but it is still negligible compared to the current obtained in presence of paracetamol in the electrolyte solution.

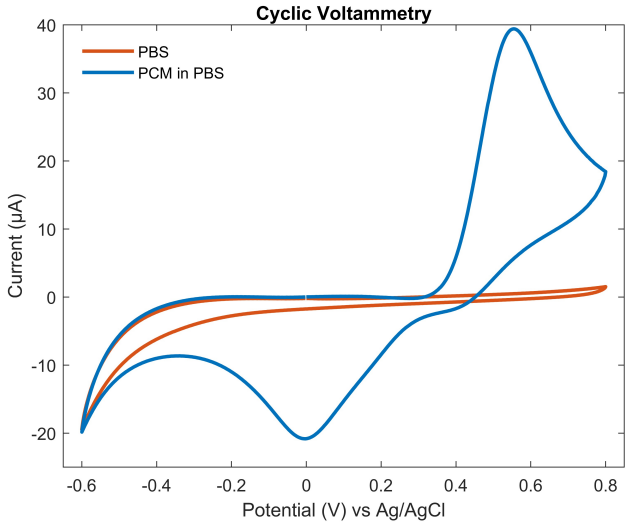

Figure 4.8: Cyclic voltammetry of $ZnFe_2O_4$ modified electrode at a fixed scan rate of 100 mV/s with 0.1 M PBS (orange) and 1.0 mM PCM in 0.1 M PBS (blue).

4.2.1 Ferrites Nanomaterials Comparison

To investigate the response of different synthesized nanomaterials in paracetamol sensing, cyclic voltammograms obtained at a fixed scan rate and with a fixed concentration of paracetamol solution were compared. Specifically, CV measurements were conducted at a scan rate of 100 mV/s with 1.0 mM of PCM in 0.1 M PBS as electrolyte solution. The comparison was made between the results obtained with the ferrite-modified sensor and the unmodified sensor.
In Figure 4.9 one scan for each type of ferrite is reported, and in Table 4.1 are reported for each material the average values of the oxidation current and the oxidation potential with the corresponding standard errors, considering 3 scans for each electrode and 3 electrodes for each material.

From Figure 4.9 and Table 4.1, the electrocatalytic action of the synthesised materials can be observed. Indeed, the bare electrode (yellow curve) is the sensor that performs worst for paracetamol detection, since its peak oxidation current

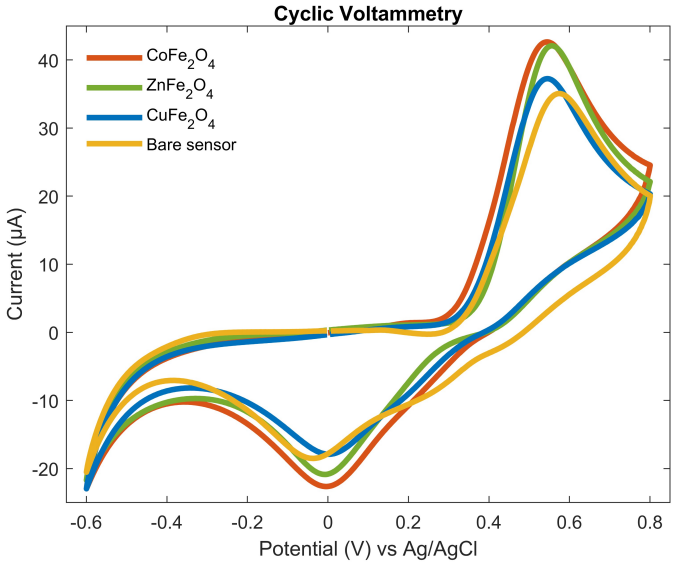

Figure 4.9: Comparison of cyclic voltammetry of bare sensor and ferrite-modified electrodes at a fixed scan rate of 100 mV/s with 1.0 mM PCM in 0.1 M PBS.

is 33.8 ± 0.1 µA. Instead, the electrode modified with copper ferrite (blue curve) shows an increase of the anodic current (35.8 ± 0.2 µA) but not as consistent as in the case of electrodes modified with cobalt ferrite (orange curve) and zinc ferrite (green curve), which exhibit more pronounced peaks of 40.1 ± 0.5 µA and 40.6 ± 0.3 µA, respectively. Furthermore, the oxidation potential of the modified sensors also shifts towards lower values compared to the bare sensor: it shifts from 577 ± 1 mV for the bare sensor to 567 ± 2 mV for $CuFe_2O_4$ sensor, 561 ± 4 mV for $CoFe_2O_4$ sensor, and 556 ± 2 mV for $ZnFe_2O_4$ sensor.
These results confirm that the synthesised ferrites act as mediators in the electron transfer occurring between the analyte and the working electrode.

Material	i_{pa} (µA)	E_{pa} (mV)
Bare sensor	33.8 ± 0.1	577 ± 1
$CuFe_2O_4$	35.8 ± 0.2	567 ± 2
$CoFe_2O_4$	40.1 ± 0.5	561 ± 4
$ZnFe_2O_4$	40.6 ± 0.3	556 ± 2

Table 4.1: Average values of oxidation peak current (i_{pa}) and oxidation potential (E_{pa}) with their respective standard errors for bare sensor and ferrite-modified electrodes for PCM detection.

4.2.2 Kinetic Analysis

To investigate the kinetics of the redox reactions occurring between the analyte and the sensor, cyclic voltammetry measurements were conducted for all materials, varying the scan rate from 50 to 300 mV/s in steps of 50 mV/s using 1.0 mM PCM in 0.1 M PBS as electrolyte solution.
The cyclic voltammograms obtained by varying the scan rate, the oxidation and reduction currents as functions of the square root of the scan rate, and the redox potentials as functions of the natural logarithm of the scan rate are shown for the bare electrode in Figure 4.10, for the $CuFe_2O_4$ modified electrode in Figure 4.11, for the $CoFe_2O_4$ modified electrode in Figure 4.12, and for the $ZnFe_2O_4$ modified electrode in Figure 4.13. Tests were conducted for all electrodes modified with each material, but only the voltammograms obtained with a single electrode modified with each material are shown. The other two graphs are obtained averaging the parameters of all the sensors modified with the same material.

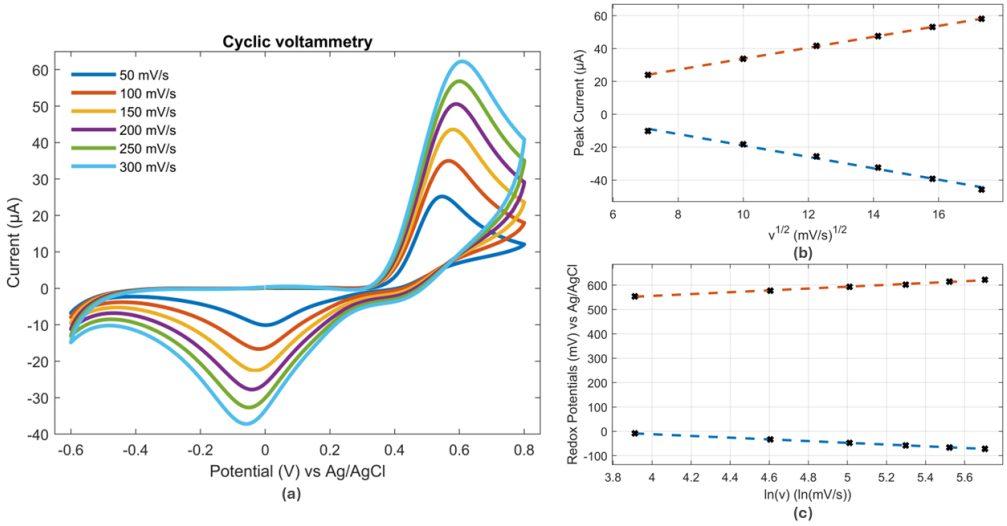

Figure 4.10: (a) Bare sensor cyclic voltammetry with 1.0 mM PCM changing the scan rate from 50 to 300 mV/s in steps of 50 mV/s. (b) Oxidation (orange) and reduction (blue) currents as a function of the root of the scan rate. (c) Oxidation (orange) and reduction (blue) potentials as a function of the natural logarithm of the scan rate.

The linear regression equations of oxidation and reduction currents as a function of the square root of the scan rate with their respective linear regression coefficients are reported in Table 4.2. The linear regression equations of oxidation and reduction potentials as a function of the natural logarithm of scan rate with their respective linear regression coefficients are shown in Table 4.3.

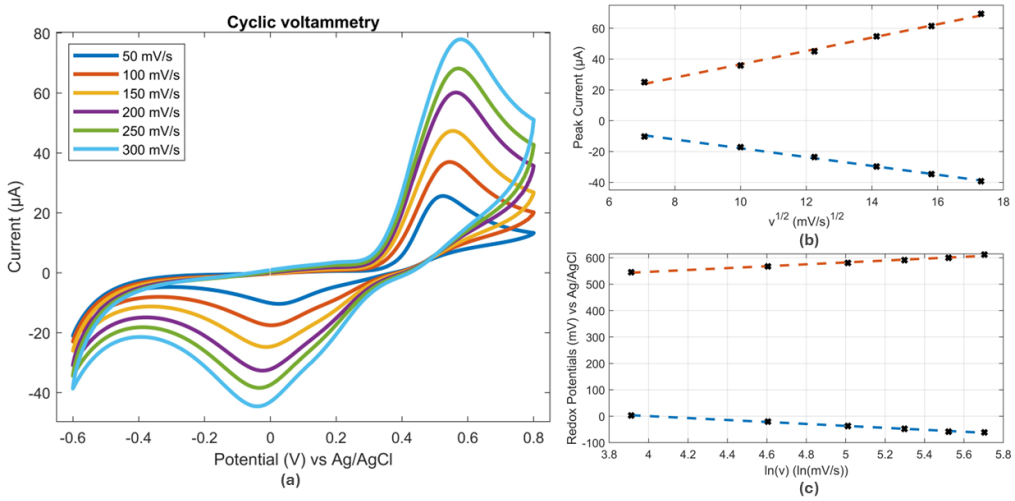

Figure 4.11: (a) $CuFe_2O_4$ modified sensor cyclic voltammetry with 1.0 mM PCM changing the scan rate from 50 to 300 mV/s in steps of 50 mV/s. (b) Oxidation (orange) and reduction (blue) currents as a function of the root of the scan rate. (c) Oxidation (orange) and reduction (blue) potentials as a function of the natural logarithm of the scan rate.

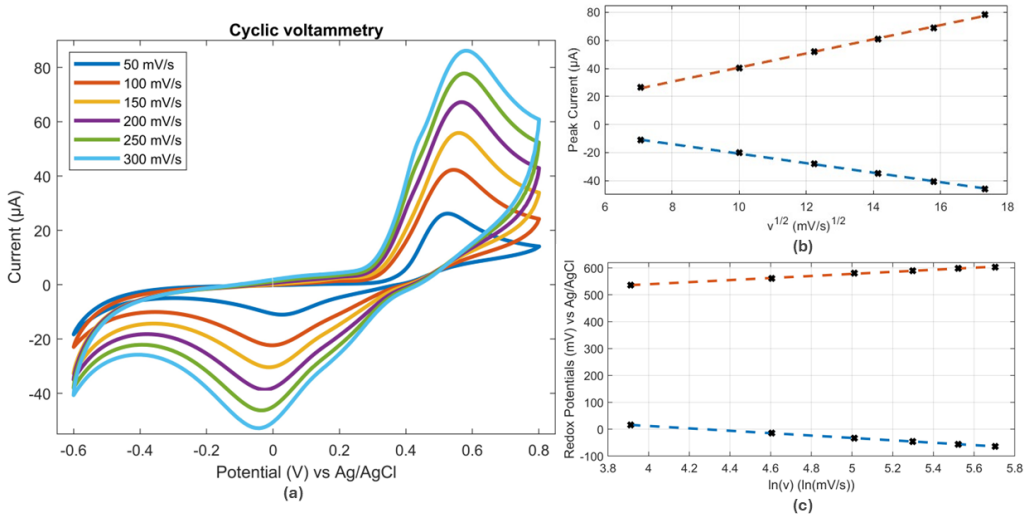

Figure 4.12: (a) $CoFe_2O_4$ modified sensor cyclic voltammetry with 1.0 mM PCM changing the scan rate from 50 to 300 mV/s in steps of 50 mV/s. (b) Oxidation (orange) and reduction (blue) currents as a function of the root of the scan rate. (c) Oxidation (orange) and reduction (blue) potentials as a function of the natural logarithm of the scan rate.

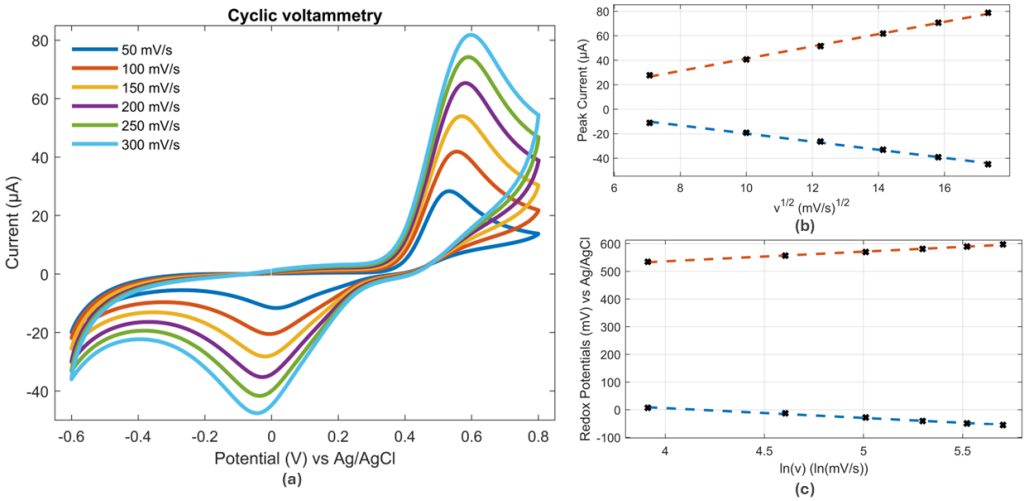

Figure 4.13: (a) $ZnFe_2O_4$ modified sensor cyclic voltammetry with 1.0 mM PCM changing the scan rate from 50 to 300 mV/s in steps of 50 mV/s. (b) Oxidation (orange) and reduction (blue) currents as a function of the root of the scan rate. (c) Oxidation (orange) and reduction (blue) potentials as a function of the natural logarithm of the scan rate.

Material	i_{pa} (µA)	R^2	i_{pc} (µA)	R^2
Bare sensor	$3.3 \cdot \sqrt{\nu} + 0.6$	0.995	$-3.5 \cdot \sqrt{\nu} + 15.8$	0.993
$CuFe_2O_4$	$4.3 \cdot \sqrt{\nu} - 6.8$	0.988	$-2.9 \cdot \sqrt{\nu} + 10.7$	0.997
$CoFe_2O_4$	$4.9 \cdot \sqrt{\nu} - 8.7$	0.997	$-3.4 \cdot \sqrt{\nu} + 12.9$	0.999
$ZnFe_2O_4$	$5.0 \cdot \sqrt{\nu} - 8.8$	0.997	$-3.3 \cdot \sqrt{\nu} + 13.3$	0.996

Table 4.2: Linear regression equations of oxidation (i_{pa}) and reduction (i_{pc}) currents as a function of the root of the scan rate with the relative linear regression coefficients (R^2) for the bare sensor and the electrodes modified with the synthesised nanomaterials for PCM detection.

For both the bare sensor and modified electrodes, the position of the redox potentials is not fixed as the scan rate varies, but shift accordingly. Additionally, the ratio between the anodic and cathodic peak currents is not unity, indicating the involvement of freely diffusing quasi-reversible systems. Consequently, these sensors can be employed for amperometric sensing applications.

Also the kinetics parameters, in particular the oxidation-reduction potential distance (ΔE_p), the electron transfer coefficient (α), the diffusion coefficient (D) and the kinetic constant rate (k), are calculated and shown in Table 4.4.

Material	E_{pa} (mV)	R^2	E_{pc} (mV)	R^2
Bare sensor	37.8·$ln(\nu)$+404.9	0.995	-35.4·$ln(\nu)$+129.8	0.999
$CuFe_2O_4$	35.7·$ln(\nu)$+401.6	0.988	-37.1·$ln(\nu)$+151.3	0.996
$CoFe_2O_4$	39.3·$ln(\nu)$+382.0	0.997	-44.5·$ln(\nu)$+190.0	0.999
$ZnFe_2O_4$	35.0·$ln(\nu)$+396.0	0.997	-35.4·$ln(\nu)$+147.4	0.998

Table 4.3: Linear regression equations of oxidation (E_{pa}) and reduction (E_{pc}) potentials as a function of the logarithm of the scan rate with the relative linear regression coefficients (R^2) for the bare sensor and the electrodes modified with the synthesised nanomaterials for PCM detection.

Material	ΔE_p (mV)	α	D (cm^2/s)	k (ms^{-1})
Bare sensor	563 ± 10	0.516 ± 0.006	$0.95 \cdot 10^{-6}$	$(28.7 \pm 5.2) \cdot 10^{-3}$
$CuFe_2O_4$	537 ± 11	0.490 ± 0.025	$1.00 \cdot 10^{-6}$	$(48.9 \pm 1.5) \cdot 10^{-3}$
$CoFe_2O_4$	515 ± 11	0.468 ± 0.015	$1.12 \cdot 10^{-6}$	$(64.1 \pm 2.2) \cdot 10^{-3}$
$ZnFe_2O_4$	507 ± 4	0.508 ± 0.012	$1.13 \cdot 10^{-6}$	$(91.7 \pm 4.0) \cdot 10^{-3}$

Table 4.4: Kinetic parameters for the bare sensor and the electrodes modified with the synthesised nanomaterials: ΔE_p peak-peak potential distance at 100 mV/s, α electron transfer coefficient, D diffusion coefficient, k kinetic constant rate for PCM detection.

The peak-to-peak separation ΔE_p reported in the table 4.4 is calculated considering a scan rate of 100 mV/s. Observing the figures, it becomes evident that ΔE_p varies and increases with the logarithm of the scan rate. Furthermore, the peak-to-peak separation of the unmodified sensor is the highest, whereas for the modified electrodes, ΔE_p is lower, with $ZnFe_2O_4$ sensor exhibiting the lowest peak-to-peak separation. This parameter is linked to the kinetics of electron transfer, indicating that the reactions occurring at the modified sensors are more likely to be reversible, resulting in lower resistance.
Moreover, as $n\Delta E_p$ in higher than 200 mV, Laviron equation can be used to calculate the electron transfer rate. The value of k at a fixed scan rate of 100 mV/s was obtained using equation 2.14 for all the electrodes. The electron transfer rate indicates the rate and efficiency of a redox reaction. Modified electrodes exhibit a higher k value, specifically 2-3 times that of the bare electrode.

4.2.3 Calibration Curves

For each material, calibration curves were obtained by plotting the oxidation current peaks obtained at the different PCM solution concentrations as a function of the paracetamol concentration. Specifically, cyclic voltammetry measurements were conducted with a constant scan rate of 100 mV/s, varying the concentration of the PCM solution from 0.5 to 3.0 mM in steps of 0.5 mM.

From the calibration curve a fundamental sensor parameter can be derived, which is the sensitivity. S is defined as the slope of the calibration curve. To obtain this parameter for each material, the average and standard error of the slopes of the three electrodes were calculated.

Limit of Detection is also a pivotal parameter of a sensor. LoD is defined as the smallest amount of analyte that can be detected and distinguished from noise. This parameter is calculated using equation 4.1

$$LoD = \frac{k \cdot \sigma}{S}, \tag{4.1}$$

where k is the statistical confidence level, S is the previously calculated sensitivity, and σ is the standard deviation of the blank CV measurement conducted without analyte, but with only PBS solution. In this study, a statistical confidence level of 3 was chosen in order to have a statistical confidence of 99.7%.

Figure 4.14 shows the CV measurements conducted by varying PCM solution concentration at a fixed scan rate of 100 mV/s, and in Figure 4.15 the calibration curves of all the sensors are reported. In Table 4.1 the equations of the calibration curves with their respective linear regression coefficients are listed. The sensitivity and the limit of detection are displayed in Table 4.6.

Material	i_{pa} (µA)	R^2
Bare sensor	24.1·[PCM]+7.0	0.986
$CuFe_2O_4$	25.7·[PCM]+7.6	0.980
$CoFe_2O_4$	25.8·[PCM]+9.0	0.976
$ZnFe_2O_4$	28.3·[PCM]+8.4	0.980

Table 4.5: Linear regression equation of the calibration curve with the relative linear regression coefficient (R^2) for the bare sensor and the electrodes modified with the synthesised nanomaterials for PCM detection.

Examining the values reported in Table 4.6, the unmodified sensor is the one with the lowest sensitivity, in fact it has a sensitivity of 24.1 ± 0.3 µA/µM. A

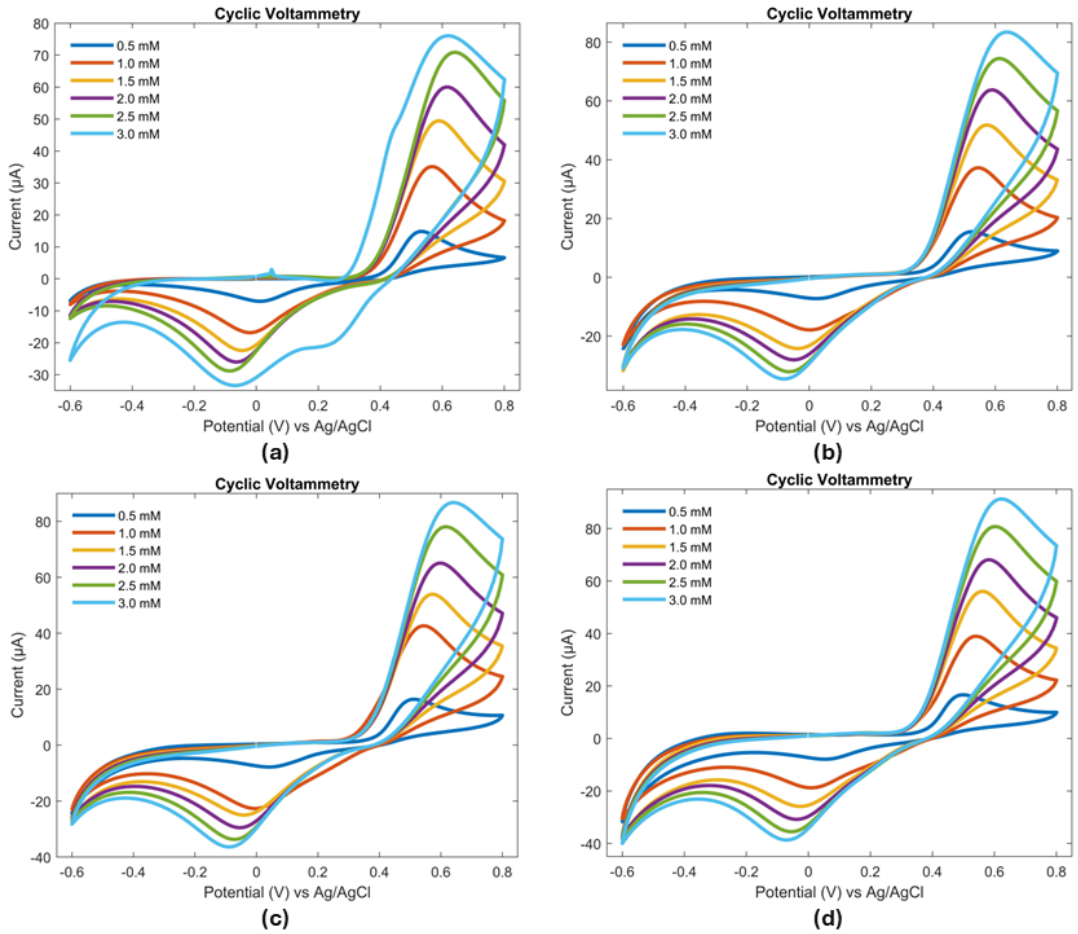

Figure 4.14: Cyclic voltammetry conducted at a fixed scan rate of 100 mV/s changing PCM solution concentration from 0.5 to 3.0 mM in steps of 0.5 mM for (a) bare sensor, (b) $CuFe_2O_4$ sensor, (c) $CoFe_2O_4$ sensor, and (d) $ZnFe_2O_4$ sensor.

Material	S ($\mu A/mM$)	LoD (μM)
Bare sensor	24.1 ± 0.3	4.4 ± 0.1
$CuFe_2O_4$	25.7 ± 0.3	3.5 ± 0.1
$CoFe_2O_4$	25.8 ± 0.6	2.3 ± 0.1
$ZnFe_2O_4$	28.3 ± 0.4	2.1 ± 0.1

Table 4.6: Sensitivity (S) and limit of detection (LoD) for the bare sensor and electrodes modified with the synthesised nanomaterials for PCM detection.

slight increase in sensitivity is observed for the sensors modified with $CuFe_2O_4$ and $CoFe_2O_4$, which have a sensitivity of 25.7 ± 0.3 µA/µM and 25.8 ± 0.6 µA/µM,

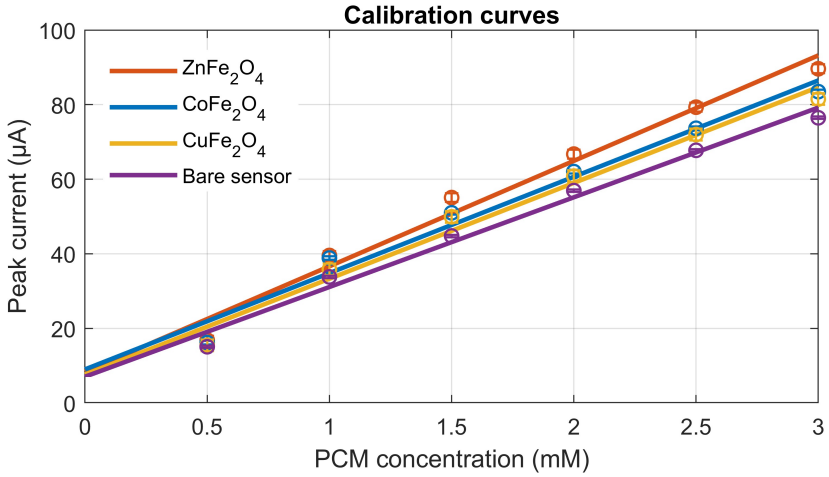

Figure 4.15: Calibration curves for the bare sensor and electrodes modified with the synthesised nanomaterials for PCM detection.

respectively. Instead, the sensor modified with $ZnFe_2O_4$ is characterized by the highest sensitivity which is equal to 28.3 ± 0.4 µA/µM.

The improvement of the detection limit is notable when ferrites are employed for sensor modification. Specifically, the unmodified sensor exhibits the highest LoD, which is equal to 4.4 ± 0.1 µM. Conversely, sensors modified with ferrites demonstrate improved LoD, with values of 3.5 ± 0.1 µM, 2.3 ± 0.1 µM, and 2.1 ± 0.1 µM for $CuFe_2O_4$, $CoFe_2O_4$, and $ZnFe_2O_4$ modified sensors, respectively. Even in terms of the limit of detection, the sensor that demonstrates superior performance is zinc ferrite modified sensor.

4.3 Cyclic Voltammetry - Cyclophosphamide

The feasibility of employing ferrites, specifically copper ferrite, as electrode modifiers for cyclophosphamide detection was explored. Inspired by Baj et al.'s work [52], electrodes modified with copper ferrite and cytochrome P450, known for its ability to reduce cyclophosphamide, were examined. Electrodes modified solely with copper ferrite, without the inclusion of cytochrome, were also tested.

4.3.1 Detection with Ferrites and Cytochrome P450

Bare electrodes and electrodes modified with copper ferrite and cytochrome P450 were tested with CV measurements for the detection of cyclophosphamide.
The experimental protocol followed is identical to that employed for paracetamol

sensing. The only varied parameters are the applied potential range, which was set between -0.6 and 0.4 V vs Ag/AgCl, and the scan rate, which was set equal to 20 mV/s, in accordance with Baj et al.'s protocol [52].
In Figure 4.16, the cyclic voltammograms depict the response of a bare sensor by varying concentration of cyclophosphamide solution. Flat signals indicate that CP exhibits no significant electrochemical behavior at these low concentrations.

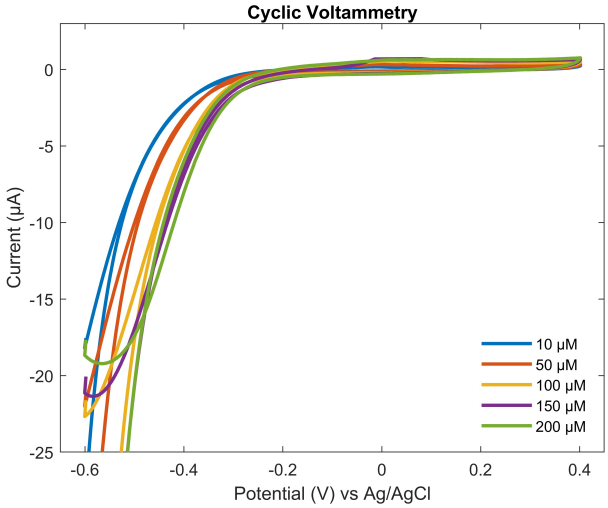

Figure 4.16: Cyclic voltammetry conducted at a fixed scan rate of 20 mV/s by varying the CP solution concentration from 10 to 200 µM for a bare sensor.

The incorporation of cytochrome becomes essential for cyclophosphamide sensing. Figure 4.17 illustrates cyclic voltammograms obtained using only 0.1 M PBS and varying CP solution concentration. By magnifying the graphs in the region of interest, i.e. around -450 mV corresponding to the reduction potential of CYP3A4 [52], subtracting the baseline (i.e. subtracting the signal obtained with 0.1 M PBS), and inverting the signal, the reduction current peaks become evident (Figure 4.18).

From the reduction current peaks obtained for various CP solution concentrations, the calibration curve, sensitivity and detection limit of the sensor can be derived. Figure 4.19 illustrates the calibration curve of the sensor, with its relative equation and linear regression coefficient provided in Table 4.7. From Table 4.8 the sensitivity of this sensor is found to be 12.7 ± 0.4 nA/µM, and 1.1 ± 0.1 nA/(µM·mm^2) considering the sensitivity normalized by the geometrical area of the working electrode. The limit of detection is equal to 11.7 ± 0.4 µM.

The results of this study align with those of Baj et al.'s work [52], in which SPEs are functionalized with MWCNTs and CYP450 for cyclophosphamide sensing. The

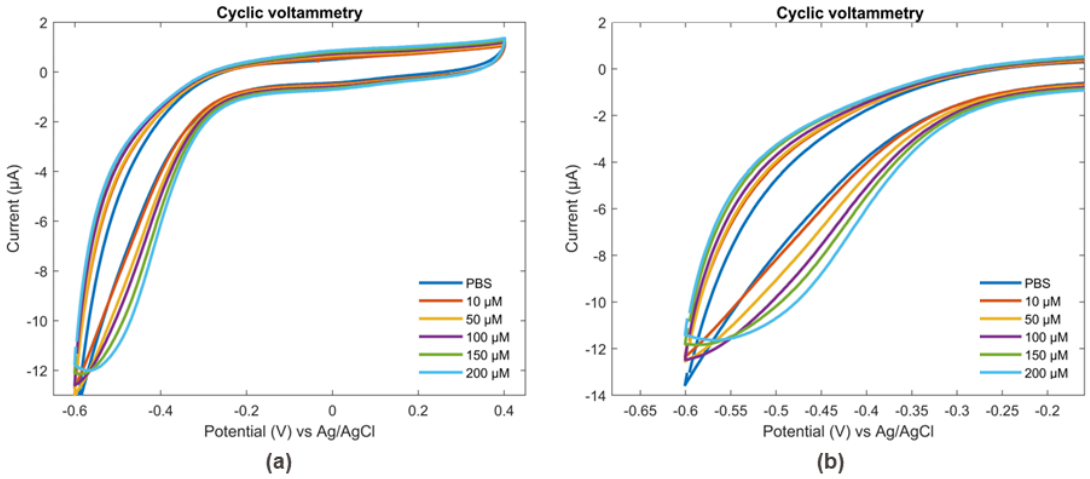

Figure 4.17: (a) Cyclic voltammetry conducted at a fixed scan rate of 20 mV/s with only 0.1 M PBS and varying CP solution concentration from 10 to 200 µM for electrode modified with $CuFe_2O_4$ and CYP3A4. (b) Zoomed-in view of cyclic voltammetry graphs in the region of interest.

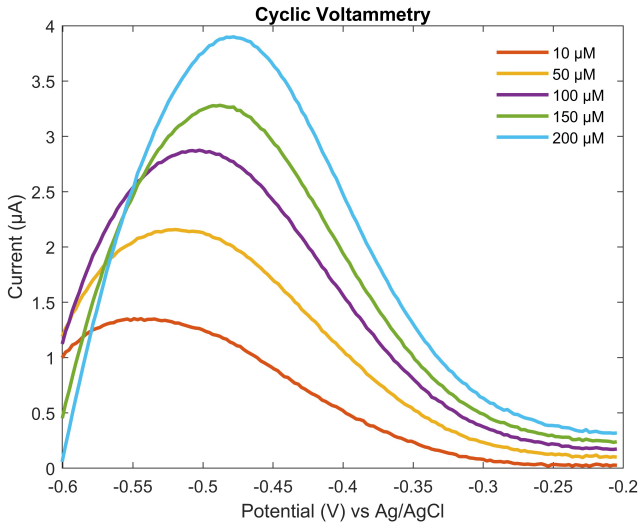

Figure 4.18: Zoomed-in view of reduction current peaks obtained at a scan rate of 20 mV/s by varying CP solution concentration from 10 to 200 µM for $CuFe_2O_4$ and CYP modified electrode after baseline subtraction and signal inversion.

sensitivity of the sensor and the response of the reduction peak exhibit a similar trend. Therefore, it is feasible to employ copper ferrite in combination with CYP450 for cyclophosphamide sensing, as an alternative to carbon nanotubes.

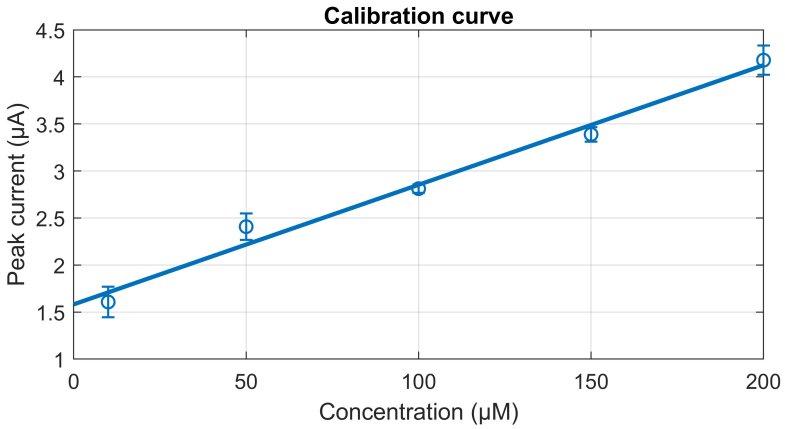

Figure 4.19: Calibration curve for the electrode modified with $CuFe_2O_4$ and CYP3A4 for CP sensing.

Material	i_{pc} (µA)	R^2
$CuFe_2O_4$ + CYP3A4	$12.7 \cdot 10^{-3} \cdot$[CP]+1.6	0.984

Table 4.7: Linear regression equation of the calibration curve with relative linear regression coefficient (R^2) for the electrode modified with $CuFe_2O_4$ and CYP3A4 for CP detection.

Material	S (nA/µM)	S_A (nA/(µM·mm^2))	LoD (µM)
$CuFe_2O_4$ + CYP3A4	12.7 ± 0.4	1.1 ± 0.1	11.7 ± 0.4

Table 4.8: Sensitivity and limit of detection for the electrode modified with $CuFe_2O_4$ and CYP3A4 for CP detection.

In this study, the concentration was varied in large steps due to the unknown electrochemical behavior of ferrite when combined with CYP450 for CP sensing. Upon examining the results, a more focused investigation within the range of CP concentrations between 10 and 70 µM with smaller steps, such as 10 µM, could be considered, as this concentration range encompasses the pharmacological levels of cyclophosphamide found in human serum [52].

4.3.2 Detection with Ferrites

Some methods have been proposed in the literature for detecting cyclophosphamide without exploiting an enzyme but through direct electron transfer [49], [58]. Hence, an attempt was made to detect cyclophosphamide using SPEs modified solely with

copper ferrite, without the incorporation of an enzyme.
Cyclic voltammetry measurements were conducted with a potential range of -0.6 to 0.4 V and a constant scan rate of 20 mV/s. An oxidation peak attributable to cyclophosphamide emerged around 100 mV (Figure 4.20).

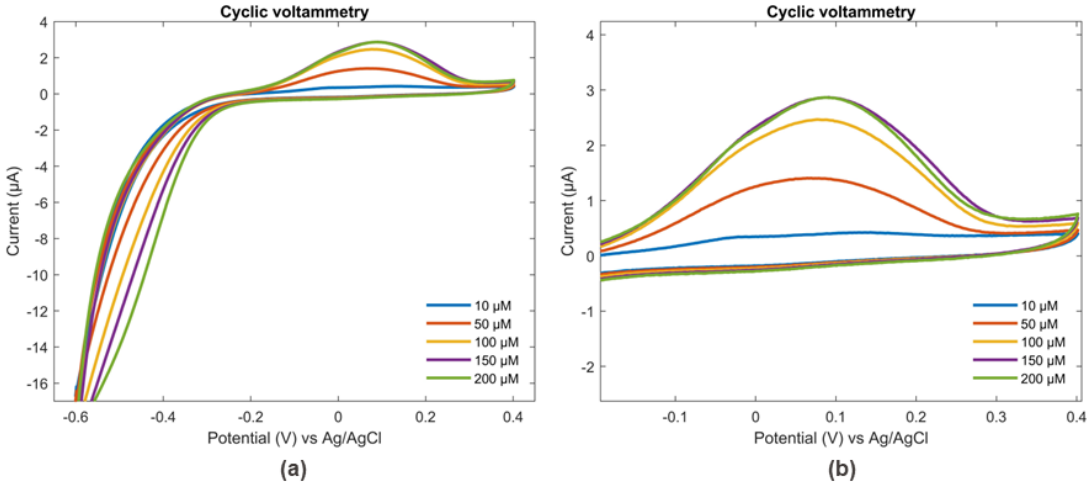

Figure 4.20: (a) Cyclic voltammetry conducted at a fixed scan rate of 20 mV/s by varying CP solution concentration from 10 to 200 µM for electrode modified with $CuFe_2O_4$. (b) Zoomed-in view of cyclic voltammetry graphs in the region of interest.

The voltammograms reveal that with an increase in the concentration of the CP solution, the saturation peak rises, but the saturation effect becomes evident. Indeed, the curves for 150 µM and 200 µM are overlapping, and the peak increase for 150 µM is less pronounced compared to smaller concentrations. Figure 4.21 (a) also shows that the concentrations of 150 µM and 200 µM are outside the linearity range. Therefore, only data collected at concentrations of 10, 50, and 100 µM were considered, as they do not demonstrate the saturation phenomenon. Moreover, the considered concentrations of cyclophosphamide solution are consistent with the therapeutic range of cyclophosphamide in human serum [52].

By focusing solely on the current peaks obtained with CP solution concentrations of 10, 50, and 100 µM, the calibration curve was derived (Figure 4.21 (b)), and the corresponding equation is presented in Table 4.9. From Table 4.10, the sensor's sensitivity and limit of detection are equal to 20.2 ± 1.3 nA/µM and 8.1 ± 0.5 µM, respectively.

Given the absence of enzyme involvement, it is possible to set a higher scan rate for varying the applied potential. Therefore, additional CV measurements were performed with a scan rate of 100 mV/s, maintaining the same potential range.

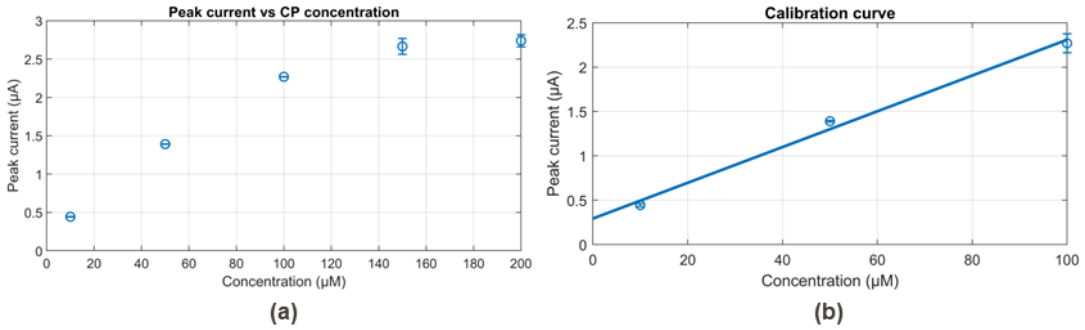

Figure 4.21: (a) Peak reduction current as a function of CP solution concentration from 10 to 200 µM for $CuFe_2O_4$ electrode at a fixed scan rate of 20 mV/s. (b) Calibration curve for $CuFe_2O_4$ electrode considering 10, 50, and 100 µM as CP solution concentrations at a fixed scan rate of 20 mV/s.

Material	i_{pc} (µA)	R^2
$CuFe_2O_4$	$20.2 \cdot 10^{-3} \cdot [CP] + 0.3$	0.993

Table 4.9: Linear regression equation of the calibration curve with relative linear regression coefficient (R^2) for $CuFe_2O_4$ electrode at a fixed scan rate of 20 mV/s for CP detection.

Material	S (nA/µM)	S_A (nA/(µM·mm^2))	LoD (µM)
$CuFe_2O_4$	20.2 ± 1.3	1.7 ± 0.1	8.1 ± 0.5

Table 4.10: Sensitivity and limit of detection for $CuFe_2O_4$ electrode at a fixed scan rate of 20 mV/s for CP detection.

The voltammograms obtained with this parameter are shown in Figure 4.22. With this scan rate an oxidation peak is still evident, but the oxidation potential has shifted to about 200 mV.

The calibration curve for this sensor was calculated (Figure 4.23), and its corresponding equation is provided in Table 4.11. The sensitivity and limit of detection were determined to be 24.3 ± 2.0 nA/µM and 6.7 ± 0.5 µM, respectively, as indicated in Table 4.12.

The sensor modified solely with copper ferrite demonstrates outstanding performance in CV measurements conducted at both 20 mV/s and 100 mV/s scan rates. The sensitivity of this sensor outperforms that of both the biosensor modified with MWCNTs and CYP450 of Baj et al.'s work [52], as well as the biosensor of this

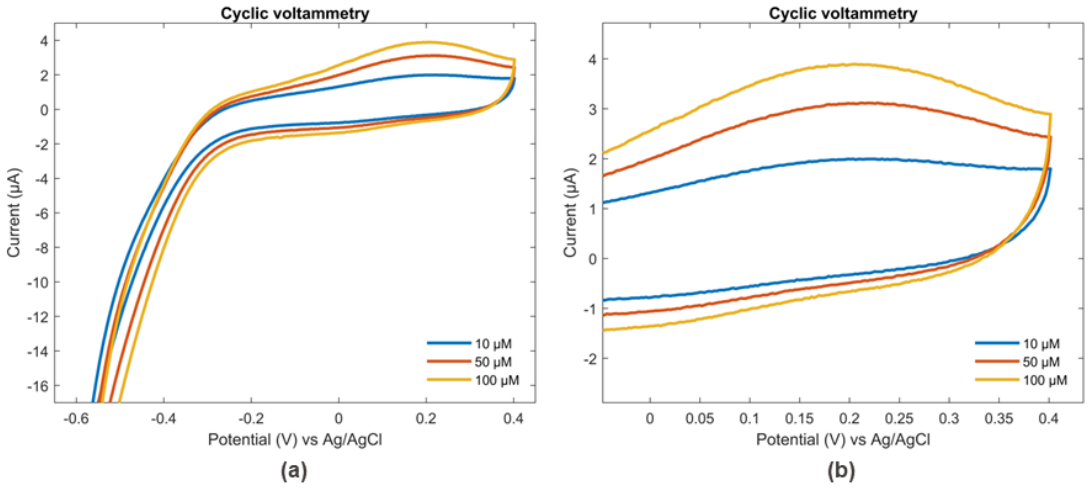

Figure 4.22: (a) Cyclic voltammetry conducted at a fixed scan rate of 100 mV/s by varying CP solution concentration from 10 to 100 µM for electrode modified with $CuFe_2O_4$. (b) Zoomed-in view of cyclic voltammetry graphs in the region of interest.

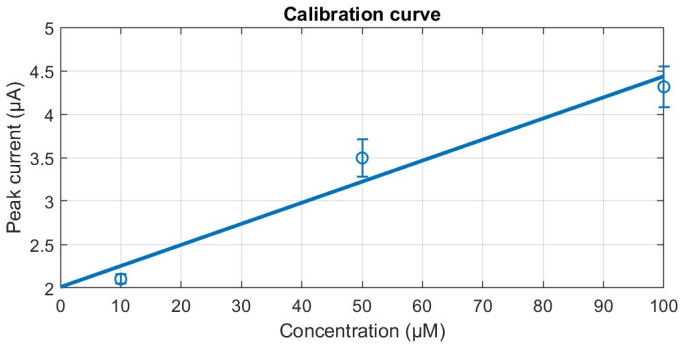

Figure 4.23: Calibration curve for $CuFe_2O_4$ electrode considering 10, 50, and 100 µM as CP solution concentration at a fixed scan rate of 100 mV/s for CP detection.

study modified with copper ferrite and CYP450. Specifically, in the case of CV measurements conducted at a scan rate of 100 mV/s, the sensor sensitivity is twice that of the other biosensors.

The achievement of successful outcomes with sensors exclusively modified with ferrites, surpassing the performance of biosensors, highlights the potential of these materials in cyclophosphamide sensing. Utilizing these materials facilitates the development of highly promising non-enzymatic sensors that exhibit stability across a wide spectrum of environmental conditions. Instead, biosensors which have enzymes as receptors demonstrate increased sensitivity to environmental factors,

Material	i_{pc} (µA)	R^2
$CuFe_2O_4$	$24.3 \cdot 10^{-3} \cdot [CP] + 2.0$	0.955

Table 4.11: Linear regression equation of the calibration curve with relative linear regression coefficient (R^2) for $CuFe_2O_4$ electrode at a fixed scan rate of 100 mV/s for CP detection.

Material	S (nA/µM)	S_A (nA/(µM·mm^2))	LoD (µM)
$CuFe_2O_4$	24.3 ± 2.0	2.0 ± 0.2	6.7 ± 0.5

Table 4.12: Sensitivity and limit of detection for $CuFe_2O_4$ electrode at a fixed scan rate of 100 mV/s for CP detection.

in particular to variations in pH and temperature, compromising long-term stability. Consequently, these non-enzymatic sensors offer the prospect of extending the operational lifespan of electrochemical biosensors, especially in the context of continuously monitoring chemical biomarkers. This becomes pivotal considering that the longevity of biosensors depends on the duration of functionality of their bio-recognition elements typically limited to a few weeks.
Moreover, the production of enzyme-based biosensors is characterized by elevated costs and the complexity of accurately immobilizing enzymes in a configuration that promotes efficient electron transfer. The modification of electrodes through the incorporation of ferrite nanoparticles emerges as a promising alternative. Employing the drop-casting technique, ferrite nanoparticles can be easily deposited onto electrode surface, creating a highly conductive substrate which promotes favorable interactions with the target analyte.

Chapter 5

Conclusions

This thesis project investigated the feasibility of incorporating nano-oxides, focusing on zinc ferrite, copper ferrite, and cobalt ferrite, in the development of non-enzymatic electrochemical sensors for the detection of pharmaceutical compounds, with a particular emphasis on paracetamol and cyclophosphamide.
Ferrites were successfully synthesized via the autocombustion method and used to functionalize the working electrodes of screen-printed carbon electrodes by the drop-casting technique, aiming to improve the sensitivity and detection capabilities of the sensors.

Cyclic voltammetry measurements were employed to analyze the sensors performance, revealing enhanced performance in detecting paracetamol compared to unmodified sensors. This indicates the role of ferrites as mediators in the electronic transfer between the electrode and the analyte. Zinc ferrite proved to be the most effective material in paracetamol sensing, showing superior performance in both kinetic parameters, such as electron transfer rate, and in sensitivity and limit of detection.

In the field of cyclophosphamide detection, unmodified sensors proved inadequate for detecting concentrations within the therapeutic range in human serum due to the absence of electrochemical behavior of cyclophosphamide itself. The incorporation of copper ferrites, either in combination with cytochrome P450 or alone, yielded remarkable results. The biosensor composed of copper ferrite and cytochrome P450 demonstrated results comparable to biosensors incorporating carbon nanotubes and cytochrome P450, considered a standard for cyclophosphamide detection. Moreover, the sensor solely composed of copper ferrite outperformed enzymatic biosensors.
Non-enzymatic sensors present several advantages, including stability under various environmental conditions, extended operating life, and an easier and more efficient manufacturing process than enzyme-based biosensors.
Despite these advantages of non-enzymatic sensors, enzyme-based sensors possess

unparalleled specificity for a specific substrate. This feature becomes particularly crucial when developing sensors capable of simultaneously detecting multiple compounds or when employed for in vivo analysis, using a biological sample as an electrolyte solution. Enzyme-based sensors offer more specific results, which is a pivotal factor in the analysis of mixtures of substances.

The promising outcomes of this project provide several prospects for future research. Optimization of ferrites synthesis could enhance uniformity, purity, and yield of nanoparticles. Exploring variations in ferrite composition, such as doping with other elements and varying element proportions, could lead to different and better properties. Extending the study to apply these sensors to other pharmaceutical compounds or clinically relevant biomolecules could expand the scope of this research in drug detection. Employing different techniques to immobilize ferrite nanoparticles on electrodes could overcome some limitations related to uniformity and thickness of the deposited material due to the drop-casting technique. Methods to enhance the specificity of non-enzymatic electrochemical sensors could be explored by implementing topological, chemical, and structural modifications. Lastly, it is essential to conduct further investigation and clarification of the surface interaction mechanisms that occur during drug sensing with these oxides.
Futher research in these directions not only contributes to a deeper understanding of nanotechnology applied to electrochemical sensors, but also promotes the development of more efficient devices for monitoring pharmaceutical compounds and clinically relevant biomolecules.

Bibliography

[1] Jaya Baranwal, Brajesh Barse, Gianluca Gatto, Gabriela Broncova, and Amit Kumar. «Electrochemical sensors and their applications: A review». In: *Chemosensors* 10.9 (2022), p. 363 (cit. on pp. 1–3).

[2] Varnakavi Naresh and Nohyun Lee. «A review on biosensors and recent development of nanostructured materials-enabled biosensors». In: *Sensors* 21.4 (2021), p. 1109 (cit. on pp. 1, 2, 5–8).

[3] Joseph R Stetter, William R Penrose, and Sheng Yao. «Sensors, chemical sensors, electrochemical sensors, and ECS». In: *Journal of The Electrochemical Society* 150.2 (2003), S11 (cit. on p. 1).

[4] Nelson R Stradiotto, Hideko Yamanaka, and Maria Valnice B Zanoni. «Electrochemical sensors: A powerful tool in analytical chemistry». In: (2003) (cit. on pp. 1–3, 5, 8).

[5] Kevin Beaver, Ashwini Dantanarayana, and Shelley D Minteer. «Materials approaches for improving electrochemical sensor performance». In: *The Journal of Physical Chemistry B* 125.43 (2021), pp. 11820–11834 (cit. on pp. 2–4, 8).

[6] Sandro Carrara. *Bio/CMOS interfaces and co-design*. Springer Nature, 2023 (cit. on pp. 2, 3).

[7] Francesca Rodino, Mattia Bartoli, and Sandro Carrara. «Simultaneous and Selective Detection of Etoposide and Methotrexate with Single Electrochemical Sensors for Therapeutic Drug Monitoring». In: *IEEE Sensors Letters* (2023) (cit. on p. 2).

[8] Dorothee Grieshaber, Robert MacKenzie, Janos Vörös, and Erik Reimhult. «Electrochemical biosensors-sensor principles and architectures». In: *Sensors* 8.3 (2008), pp. 1400–1458 (cit. on pp. 2–4).

[9] Jae Hyun Kim, Young Joon Suh, Dongsung Park, Hyoju Yim, Hongrae Kim, Hye Jin Kim, Dae Sung Yoon, and Kyo Seon Hwang. «Technological advances in electrochemical biosensors for the detection of disease biomarkers». In: *Biomedical Engineering Letters* 11.4 (2021), pp. 309–334 (cit. on p. 2).

[10] Giti Paimard, Ehsan Ghasali, and Mireia Baeza. «Screen-Printed Electrodes: Fabrication, Modification, and Biosensing Applications». In: *Chemosensors* 11.2 (2023), p. 113 (cit. on p. 3).

[11] Ricarda Torre, Estefanía Costa-Rama, Henri PA Nouws, and Cristina Delerue-Matos. «Screen-printed electrode-based sensors for food spoilage control: Bacteria and biogenic amines detection». In: *Biosensors* 10.10 (2020), p. 139 (cit. on p. 3).

[12] Keiichiro Yamanaka, Mun'delanji C Vestergaard, and Eiichi Tamiya. «Printable electrochemical biosensors: A focus on screen-printed electrodes and their application». In: *Sensors* 16.10 (2016), p. 1761 (cit. on p. 3).

[13] Shreanshi Agrahari, Ankit Kumar Singh, Ravindra Kumar Gautam, and Ida Tiwari. «Electrochemical oxidation and sensing of para benzoquinone using a novel SPE based disposable sensor». In: *Chemosphere* 342 (2023), p. 140078 (cit. on p. 3).

[14] Fabiana Arduini, Fabio Di Nardo, Aziz Amine, Laura Micheli, Giuseppe Palleschi, and Danila Moscone. «Carbon black-modified screen-printed electrodes as electroanalytical tools». In: *Electroanalysis* 24.4 (2012), pp. 743–751 (cit. on p. 3).

[15] Antonio Rubino and Raquel Queirós. «Electrochemical determination of heavy metal ions applying screen-printed electrodes based sensors. A review on water and environmental samples analysis». In: *Talanta Open* (2023), p. 100203 (cit. on p. 3).

[16] Zahra Taleat, Alireza Khoshroo, and Mohammad Mazloum-Ardakani. «Screen-printed electrodes for biosensing: A review (2008-2013)». In: *Microchimica Acta* 181 (2014), pp. 865–891 (cit. on pp. 4–6).

[17] M Ramya, P Senthil Kumar, Gayathri Rangasamy, G Rajesh, K Nirmala, A Saravanan, Alagumalai Krishnapandi, et al. «A recent advancement on the applications of nanomaterials in electrochemical sensors and biosensors». In: *Chemosphere* (2022), p. 136416 (cit. on pp. 4, 8, 9).

[18] I Moldoveanu, RI van Stefan-Staden, JF van Staden, M Aliofkhazraei, and A Makhlouf. «Electrochemical sensors based on nanostructured materials». In: *Handbook of Nanoelectrochemistry: Electrochemical Synthesis Methods, Properties and Characterization Techniques* (2016), pp. 1–15 (cit. on pp. 4, 8).

[19] Celine IL Justino, Teresa A Rocha-Santos, and Armando C Duarte. «Review of analytical figures of merit of sensors and biosensors in clinical applications». In: *TrAC Trends in Analytical Chemistry* 29.10 (2010), pp. 1172–1183 (cit. on p. 4).

[20] George S Wilson and Raeann Gifford. «Biosensors for real-time in vivo measurements». In: *Biosensors and Bioelectronics* 20.12 (2005), pp. 2388–2403 (cit. on p. 4).

[21] Bansi D Malhotra, Rahul Singhal, Asha Chaubey, Sandeep K Sharma, and Ashok Kumar. «Recent trends in biosensors». In: *Current Applied Physics* 5.2 (2005), pp. 92–97 (cit. on p. 5).

[22] O Dominguez Renedo, MA Alonso-Lomillo, and MJ Arcos Martinez. «Recent developments in the field of screen-printed electrodes and their related applications». In: *Talanta* 73.2 (2007), pp. 202–219 (cit. on p. 5).

[23] Eun-Hyung Yoo and Soo-Youn Lee. «Glucose biosensors: an overview of use in clinical practice». In: *Sensors* 10.5 (2010), pp. 4558–4576 (cit. on p. 6).

[24] Chorom Jang, Hee-Jo Lee, and Jong-Gwan Yook. «Radio-frequency biosensors for real-time and continuous glucose detection». In: *Sensors* 21.5 (2021), p. 1843 (cit. on pp. 6, 7).

[25] Won-Yong Jeon, Han-Sem Kim, Hye-Won Jang, Ye-Sung Lee, Ueon Sang Shin, Hyug-Han Kim, and Young-Bong Choi. «A stable glucose sensor with direct electron transfer, based on glucose dehydrogenase and chitosan hydro bonded multi-walled carbon nanotubes». In: *Biochemical Engineering Journal* 187 (2022), p. 108589 (cit. on pp. 6, 7).

[26] Omotayo Adeniyi, Nnamdi Nwahara, Daniel Mwanza, Tebello Nyokong, and Philani Mashazi. «High-performance non-enzymatic glucose sensing on nanocomposite electrocatalysts of nickel phthalocyanine nanorods and nitrogen doped-reduced graphene oxide nanosheets». In: *Applied Surface Science* 609 (2023), p. 155234 (cit. on p. 7).

[27] Dayakar Thatikayala, Deepalekshmi Ponnamma, Kishor Kumar Sadasivuni, John-John Cabibihan, Abdulaziz Khalid Al-Ali, Rayaz A Malik, and Booki Min. «Progress of advanced nanomaterials in the non-enzymatic electrochemical sensing of glucose and H2O2». In: *Biosensors* 10.11 (2020), p. 151 (cit. on p. 7).

[28] Bhaskara V Chikkaveeraiah, Ashwinkumar A Bhirde, Nicole Y Morgan, Henry S Eden, and Xiaoyuan Chen. «Electrochemical immunosensors for detection of cancer protein biomarkers». In: *ACS nano* 6.8 (2012), pp. 6546–6561 (cit. on p. 7).

[29] Zhenguo Zhang, Yulin Cong, Yichun Huang, and Xin Du. «Nanomaterials-based electrochemical immunosensors». In: *Micromachines* 10.6 (2019), p. 397 (cit. on p. 7).

[30] Corinne Dejous and Uma Maheswari Krishnan. «Sensors for diagnosis of prostate cancer: Looking beyond the prostate specific antigen». In: *Biosensors and Bioelectronics* 173 (2021), p. 112790 (cit. on p. 8).

[31] Sajjad Hussain et al. «Synthesis and characterization of vanadium ferrites, electrochemical sensing of acetaminophen in biological fluids and pharmaceutical samples». In: *Ceramics International* 49.5 (2023), pp. 8165–8171 (cit. on pp. 8, 12, 13).

[32] Isabela Jasper, Tatiana Lima Valério, Vanessa Klobukoski, Camila Melo Pesqueira, Jonas Massaneiro, Luan Pereira Camargo, Luiz Henrique Dall' Antonia, and Marcio Vidotti. «Electrocatalytic and Photoelectrocatalytic Sensors Based on Organic, Inorganic, and Hybrid Materials: A Review». In: *Chemosensors* 11.5 (2023), p. 261 (cit. on p. 9).

[33] Rohit Ranga, Ashok Kumar, Parveen Kumari, Permender Singh, Vasundhara Madaan, and Krishan Kumar. «Ferrite application as an electrochemical sensor: A review». In: *Materials Characterization* 178 (2021), p. 111269 (cit. on p. 9).

[34] António B Mapossa, Washington Mhike, José L Adalima, and Shepherd Tichapondwa. «Removal of organic dyes from water and wastewater using magnetic ferrite-based titanium oxide and zinc oxide nanocomposites: a review». In: *Catalysts* 11.12 (2021), p. 1543 (cit. on p. 10).

[35] Josué Gonçalves, Lucas de Faria, Amanda Nascimento, Rafael Germscheidt, Santanu Patra, Lucas Hernández-Saravia, Juliano Bonacin, Rodrigo Munoz, and Lúcio Angnes. «Sensing performances of spinel ferrites MFe2O4 (M= Mg, Ni, Co, Mn, Cu and Zn) based electrochemical sensors: A review». In: *Analytica Chimica Acta* 1233 (2022), p. 340362 (cit. on pp. 9–11, 25).

[36] Kebede K Kefeni, Titus AM Msagati, and Bhekie B Mamba. «Ferrite nanoparticles: synthesis, characterisation and applications in electronic device». In: *Materials Science and Engineering: B* 215 (2017), pp. 37–55 (cit. on pp. 10, 11).

[37] Mallikarjun Madagalam, Mattia Bartoli, Michele Rosito, Nicola Blangetti, Marco Etzi Coller Pascuzzi, Elisa Padovano, Barbara Bonelli, Sandro Carrara, and Alberto Tagliaferro. «Unraveling the Effect of the Chemical and Structural Composition of Zn x Ni1- x Fe2O4 on the Electron Transfer at the Electrochemical Interface». In: *Small Structures* 4.12 (2023), p. 2300163 (cit. on pp. 10, 23, 25, 31, 32).

[38] Thomas Dippong, Erika Andrea Levei, and Oana Cadar. «Recent advances in synthesis and applications of MFe2O4 (M= Co, Cu, Mn, Ni, Zn) nanoparticles». In: *Nanomaterials* 11.6 (2021), p. 1560 (cit. on p. 11).

[39] S-H Feng and G-H Li. «Hydrothermal and solvothermal syntheses». In: *Modern inorganic synthetic chemistry*. Elsevier, 2017, pp. 73–104 (cit. on p. 11).

[40] Farzana Majid, Javeria Rauf, Sadia Ata, Ismat Bibi, Abdul Malik, Sobhy M Ibrahim, Adnan Ali, and Munawar Iqbal. «Synthesis and characterization of NiFe2O4 ferrite: Sol–gel and hydrothermal synthesis routes effect on magnetic, structural and dielectric characteristics». In: *Materials Chemistry and Physics* 258 (2021) (cit. on p. 11).

[41] Morassa Hassannezhad, Morteza Hosseini, Mohammad Reza Ganjali, and Majid Arvand. «Electrochemical sensor based on carbon nanotubes decorated with ZnFe2O4 nanoparticles incorporated carbon paste electrode for determination of metoclopramide and indomethacin». In: *ChemistrySelect* 4.25 (2019), pp. 7616–7626 (cit. on p. 11).

[42] Dina F Katowah, Mohammed M Rahman, Mahmoud A Hussein, TR Sobahi, MA Gabal, MM Alam, and Abdullah M Asiri. «Ternary nanocomposite based poly (pyrrole-co-O-toluidine), cobalt ferrite and decorated chitosan as a selective Co2+ cationic sensor». In: *Composites Part B: Engineering* 175 (2019), p. 107175 (cit. on p. 11).

[43] Chuan-Ling Zhang and Shu-Hong Yu. «Nanoparticles meet electrospinning: recent advances and future prospects». In: *Chemical Society Reviews* 43.13 (2014), pp. 4423–4448 (cit. on p. 11).

[44] Mallikarjun Madagalam, Mattia Bartoli, Sandro Carrara, Alberto Tagliaferro, et al. «ZnCr2-xFexO4 Nanoparticles-Modified Electrochemical Sensors: A Comparative Study». In: *2023 IEEE SENSORS*. IEEE, 2023 (cit. on p. 12).

[45] Anitha Kumary Vidyadharan, Divya Jayan, and TE Mary Nancy. «Ni0.1Co0.9 Fe2O4-based electrochemical sensor for the detection of paracetamol». In: *Journal of Solid State Electrochemistry* 18.9 (2014), pp. 2513–2519 (cit. on p. 12).

[46] Lanting Qian, Sharmila Durairaj, Scott Prins, and Aicheng Chen. «Nanomaterial based electrochemical sensors and biosensors for the detection of pharmaceutical compounds». In: *Biosensors and Bioelectronics* 175 (2021) (cit. on p. 12).

[47] Wafaa Boumya, Nawal Taoufik, Mounia Achak, and Noureddine Barka. «Chemically modified carbon-based electrodes for the determination of paracetamol in drugs and biological samples». In: *Journal of Pharmaceutical Analysis* 11.2 (2021), pp. 138–154 (cit. on p. 13).

[48] Yogendra Kumar, Panchanan Pramanik, and Dipak Kumar Das. «Electrochemical detection of paracetamol and dopamine molecules using nanoparticles of cobalt ferrite and manganese ferrite modified with graphite». In: *Heliyon* 5.7 (2019) (cit. on p. 13).

[49] Bintong Huang, Lili Xiao, Haifeng Dong, Xueji Zhang, Wei Gan, Shahid Mahboob, Khalid Abdullah Al-Ghanim, Qunhui Yuan, and Yingchun Li. «Electrochemical sensing platform based on molecularly imprinted polymer decorated N, S co-doped activated graphene for ultrasensitive and selective determination of cyclophosphamide». In: *Talanta* 164 (2017), pp. 601–607 (cit. on pp. 13, 47).

[50] Uttpal Anand et al. «Cancer chemotherapy and beyond: Current status, drug candidates, associated risks and progress in targeted therapeutics». In: *Genes & Diseases* (2022) (cit. on p. 13).

[51] Camilla Baj-Rossi, Giovanni De Micheli, and Sandro Carrara. *P450-based nano-bio-sensors for personalized medicine*. Vol. 21. Chapter, 2011 (cit. on p. 14).

[52] Camilla Baj-Rossi, Giovanni De Micheli, and Sandro Carrara. «Electrochemical detection of anti-breast-cancer agents in human serum by cytochrome P450-coated carbon nanotubes». In: *Sensors* 12.5 (2012), pp. 6520–6537 (cit. on pp. 14, 44, 45, 47–49).

[53] Noémie Elgrishi, Kelley J Rountree, Brian D McCarthy, Eric S Rountree, Thomas T Eisenhart, and Jillian L Dempsey. «A practical beginner's guide to cyclic voltammetry». In: *Journal of chemical education* 95.2 (2018), pp. 197–206 (cit. on pp. 17, 20, 21).

[54] Laviron. «General expression of the linear potential sweep voltammogram in the case of diffusionless electrochemical systems». In: *Journal of Electroanalytical Chemistry and Interfacial Electrochemistry* 101.1 (1979), pp. 19–28 (cit. on p. 22).

[55] Ruchita S Das and YK Agrawal. «Raman spectroscopy: Recent advancements, techniques and applications». In: *Vibrational spectroscopy* 57.2 (2011), pp. 163–176 (cit. on p. 31).

[56] Raghvendra Singh Yadav, Jaromir Havlica, Jiri Masilko, Lukas Kalina, Jaromir Wasserbauer, Miroslava Hajdúchová, Vojtěch Enev, Ivo Kuřitka, and Zuzana Kožáková. «Cation migration-induced crystal phase transformation in copper ferrite nanoparticles and their magnetic property». In: *Journal of Superconductivity and Novel Magnetism* 29 (2016), pp. 759–769 (cit. on pp. 31, 32).

[57] Raghvendra Singh Yadav et al. «Impact of grain size and structural changes on magnetic, dielectric, electrical, impedance and modulus spectroscopic characteristics of CoFe2O4 nanoparticles synthesized by honey mediated sol-gel combustion method». In: *Advances in Natural Sciences: Nanoscience and Nanotechnology* 8.4 (2017) (cit. on pp. 31, 32).

[58] P Palaska, E Aritzoglou, and S Girousi. «Sensitive detection of cyclophosphamide using DNA-modified carbon paste, pencil graphite and hanging mercury drop electrodes». In: *Talanta* 72.3 (2007), pp. 1199–1206 (cit. on p. 47).

Acknowledgements

Al termine di questo percorso, vorrei ringraziare tutte le persone che hanno contribuito a rendere questa esperienza indimenticabile.

Innanzitutto, ringrazio i professori Alberto e Sandro, che mi hanno dato l'opportunità di intraprendere questo progetto e che mi hanno accolta nei loro gruppi di ricerca.
Ringrazio Mattia, per avermi seguita in modo costante durante tutto il progetto di tesi, soprattutto nel periodo in Svizzera, e per aver sempre risposto alle mie mille domande.
Ringrazio gli amici del gruppo di ricerca BCI dell'EPFL e del Carbon Group del Poli, con i quali ho condiviso questo viaggio. Le pause caffè, le cene, le nostre risate e i nostri pianti hanno reso questa esperienza ricca di colore.

Ringrazio la mia famiglia per il costante sostegno, soprattutto durante questi anni trascorsi lontano da casa.
Ringrazio Simone per essere stato sempre al mio fianco e per avermi supportata.
Ringrazio tutti gli amici che ho incontrato lungo questo percorso e con i quali ho condiviso questi anni di gioie e di sfide.

Tutti voi avete contribuito a rendermi la persona che sono oggi.